# Advanced Power Oscillation Damping for a Wind Power Plant


Asger Nickelsen

FACULTY OF ENGINEERING AND SCIENCE



MSc. in Electrical Power Systems and High Voltage,

Submission date 02/08/2021


Master Thesis

STUDENT REPORT

AALBORG UNIVERSITY

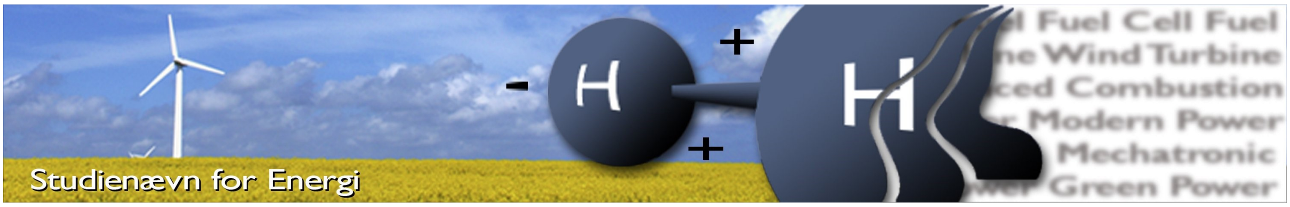


**Title:**

**Semester:** 10'th
**Semester theme:**

**Project period:** 01.02.2021 to 28.05.2021
**ECTS:** 30
**Supervisor:** Florin Iov
**Co-supervisor:** Germán Claudio Tarnowski
**Project group:** EPSH4-1036.


**Group members:**
Asger Nickelsen


| | |
|---|---|
| Total: | 86 pages |
| Appendix: | 6 pages |
| supplement: | none |


**Synopsis**

Worldwide the energy sector is moving towards a greener and more sustainable future by integrating more renewable based generation plants while decommissioning conventional generation units. As a result the power grid is seeing a decrease in system inertia and is becoming more susceptible to power oscillations. Power systems stabilizers were used in conventional power plants control schemes to mitigate these oscillations. Therefore, in order to maintain the stability and security of power supply the renewable generation plants should be able to provide similar capabilities. This project is investigating and proposing a feasible mitigation methods for the power system oscillations implemented in wind turbines and/or at wind power plants. These methods should be easily applied worldwide on various grid connection characteristics by wind turbine manufactures and plant owners. The proposed methods should also provide effective damping to power grid while not endangering the operation of the wind turbines.


**By accepting the request from the fellow student who uploads the study group's project report in Digital Exam System, you confirm that all group members have participated in the project work, and thereby all members are collectively liable for the contents of the report. Furthermore, all group members confirm that the report does not include plagiarism.**

# Summary

To reach the climate goal of keeping the world temperature from rising more than 2° green energy solutions are on the rise simultaneously as traditional power generation is being retired. Specifically, solutions from off-shore wind power parks are seeing an increase in commotions in the north sea of the European Union. However, this development faces some challenges, one is the available power in the power grid is becoming more dependent on local weather phenomenons, another challenge is the power grid with the retirement of traditional power generation is seeing a decrease in available inertia in the system. It is the later challenge that is being focused on in this project by investigating if wind power plants can participate in power oscillation damping as low inertia systems are more prone to power oscillations, which can cause power system blackouts. However, worldwide it appears that current grid codes have not been developed for allowing wind power plants to provide this type of control, meaning the industry does not have any design criteria to follow. Therefore does this report attempts to establish a set of practical design criteria that can serve as a baseline. The report investigates this through a literature study to map out current solutions from literature, whereafter it adopts a solution and develops a POD controller that can be incorporated into the reactive power control loop of a main controller for the wind power plant. The report then investigates how the current danish grid codes affect the performance of the chosen controller solution and evaluate if it is possible to acquire adequate damping while remaining inside grid codes limitation through simulation and validation of the controller in Mathworks Simulink. From these investigations, it has been found that it was not possible to acquire adequate damping while upholding the grid codes issue by the Danish TSO Energinet. However, it was also concluded that damping can be achieved if the grid codes are adjusted to allow for a higher ramping rate than currently allowed by the codes. But it was also found that with the adjustment it was still not possible to achieve adequate damping. Therefore do the report conclude that damping is possible with the developed controller, however, further research is needed on the topic in order to establish some more elaborate design criteria to develop controller designs after. Similarly, it is concluded that only a partial answer to the problem formulation was achieved as the performance of the controller has only been tested for single-frequency warranting additional testing of the POD controller.

# Preface

This master thesis has been produced by Asger Nickelsen a 4'th semester master student at the department of energy technology at Aalborg University, in collaboration with supervisor Florin Iov and co-supervisor Germán Claudio Tarnowski. The focus of the project has been on developing and proposing a set of practical design criteria for developing a power oscillation damping controller for off-shore wind power plants.

I would like to extend a special thanks to my supervisor Florin Iov for showing endless patients with my endless questions, and thanks to Germán Claudio Tarnowski for coming with inputs from the industry perspective.

## Readers' Guide

citations are stated using the Vancouver method, i.e. [cite number, page]. The bibliography is located at the end of the report, where websites are denoted "author, title, URL, year of publication and last visited in dd/mm/yy". Books are denoted "author, title, publisher, edition, year of publication, year of reprint and ISBN" and technical reports are denoted "author, title, institution and year". Note, the placement of the citation determines which part of the text it refers to, as illustrated:

| | | |
|---|---|---|
| [1, p. 1]. | *Before period* | Refers to sentence. |
| . [1, p. 1] | *After period* | Refers to section. |

Captions for figures and tables are denoted by the chapter number and figure/table number below the given figure or table. E.g. figure 2 in chapter 4 will be referred to as "Figure 4.2". Similarly, equations are denoted with the chapter- and equation number to the right hand side of the equation. E.g. equation 7 in chapter 4, is referenced as "Equation (4.7)".

Appendixes are located after the bibliography in the end of the report and are listed alphabetically. The appendixes contain a single line diagram of the utilised PowerFactory system, WTG modelling parameters, the calculated NVSI indices for the intact grid, voltage graphs, scatter plots as well as MATLAB and python scripts.

# Nomenclature

## Symbols

| Symbol | Name | Unit |
|---|---|---|
| $\delta$ | Angle | ° |
| $\Delta$ | Difference | - |
| ° | degrees | ° |
| $\zeta$ | damping coefficient | - |
| $\omega$ | angular speed | - |
| f | frequency | Hertz |
| I | Current | A |
| K | gain constant | - |
| P | Active power | W |
| Q | Reactive power | VAr |
| R | Resistance | Ω |
| S | Apparent power | VA |
| s | laplace operator | - |
| T | Time Constant | - |
| T | Torque | Nm |
| V | voltage | V |
| X | reactance | Ω |
| $Z$ | Impedance | Ω |
| 1,2,3,... | index number | - |

## Subscripts

| Symbol | Name |
|---|---|
| e | electrical |
| eq | equivalent |
| G/g | Grid |
| l | line |

| | |
|---|---|
| LL | line to line |
| n | natural |
| meas | measurement |
| k | Rated Power |
| s | Stability Signal |
| SC | Short Circuit |
| t | terminal |
| r | rotor |
| ref | reference |
| w | Washout |
| WPP | Wind Power park |

# Abbreviations

| **Abbreviation** | **Definition** |
|---|---|
| AAU | Aalborg University |
| AC | Alternating Current |
| AVR | Automatic Voltage Regulator |
| APC | Absolute Power Constraint |
| AQR | Automatic Reactive Power Regulator |
| AUX | Auxiliary |
| CE | Continental Europe |
| CHP | Combined Heat and Power |
| DC | Direct Current |
| DFIG | Doubly Fed Induction Generator |
| DPC | Delta Power Constraint |
| EPON | Ethernet Passive Optical Network |
| FACTS | Flexible AC Transmission System |
| FC | Frequency Control |
| FMAC | Flux Magnitude and Angle Control |
| FR | Frequency Response |
| HV | High Voltage |
| HVDC | High Voltage Direct Current |
| IEC | International Electrotechnical Commission |
| IEEE | Institute of Electrical and Electronics Engineers |

| | |
|---|---|
| OPPT | Optimized Power Point Tracking |
| PED | Power Electronic Device |
| PEIPS | Power Electronic Interface Power Sources |
| PFC | Power Factor Control |
| PMSG | Permanent Magnet Synchronous Generator Wind Turbine |
| PO | Power Oscillation |
| POC | Point of Connection |
| PPC | Point of Common Coupling |
| PPM | Power Park Module |
| POD | Power Oscillation Damping |
| PV | Photo Voltaic |
| PSS | Power System Stabiliser |
| PWM | Pulse Width Modulation |
| QC | Reactive Power Control |
| RE | Renewable Energy |
| RES | Renewable Energy Source |
| RMS | Root Mean Square |
| RRC | Ramp Rate Constraint |
| SC | Short Circuit |
| SCR | Short Circuit Ratio |
| SVC | Static VAR Compensator |
| SG | Synchronous Generator |
| TSO | Transmission System Operator |
| UK | United Kingdom |
| VC | Voltage Control |
| WAMS | Wide Area Measurement Systems |
| WTG | Wind Turbine Generator |
| WPP | Wind Power Park |
| WT | Wind Turbine |

# Table of Contents

# 1 Introduction

This chapter will outline the current trend in Continental Europe (CE) with regards to new commissions of Renewable Energy Sources (RES) and highlight what challenges the Transmission Operators (TSO) are expected to see in the future with a high penetration of RES. Lastly, the chapter will introduce the different Power Oscillation (PO) modes observed in the CE power grid, and the solutions utilized to dampen them.

## 1.1 Climate Goals

Worldwide the energy sector is moving towards a greener energy sector, by integrating RES. This change in the energy sector is highly motivated by political goals to reduce $CO_2$ emissions to reduce humanity's impact on climate change, and preventing the world temperature from rising more than 2°C. An example of such a legislative body is the European Parliament, which has set a goal for reducing the $CO_2$ emission by 55% by 2030 compared to what was emitted in 1990, The 2030 goal is a partial goal in the plan to reach climate neutrality by 2050 [2]. This goal of 55% reduction in $CO_2$ has caused an increase in the commissioning of new RES.

The Northern European countries are seeing an increase in their offshore wind power capacity. This is seen when investigating installed wind power capacity in the Northern European countries, as the power capacity from offshore wind power plants in 2020 rose by 2.901 [MW]. Wind Power Plant (WPP) power capacity from offshore wind is distributed between the Netherlands (1.493 [MW]), Belgium (706[MW]), the UK (483 [MW]), and Germany (219 [MW]). Due note Portugal's contribution with 17 [MW] have not been included, as it is not considered a Northern European country.[3, p. 7]

To highlight the development in offshore wind power the increase in the commissioned WPPs over the past 10 years from 2010 to 2020 is illustrated in Figure 1.1. It is clear that the annual installed capacity of offshore wind power haven been annually increasing in Europe over the past 10 years indicated with the red curve in Figure 1.1 .[3, p. 6]

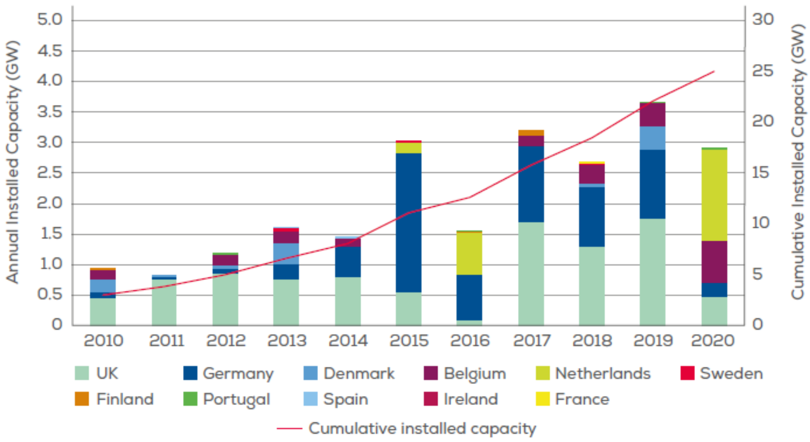


Figure 1.1: Installed offshore wind power capacity from 2010 to 2020.[3, p. 6]

Observing Figure 1.2 it is seen that the penetration of offshore wind power is higher in the northern part of Europe. Where the countries of the UK, Germany, Netherlands Belgium, and Denmark make up 99% of the installed capacity, with 79% of the capacity installed in the North Sea. [3, p. 14]

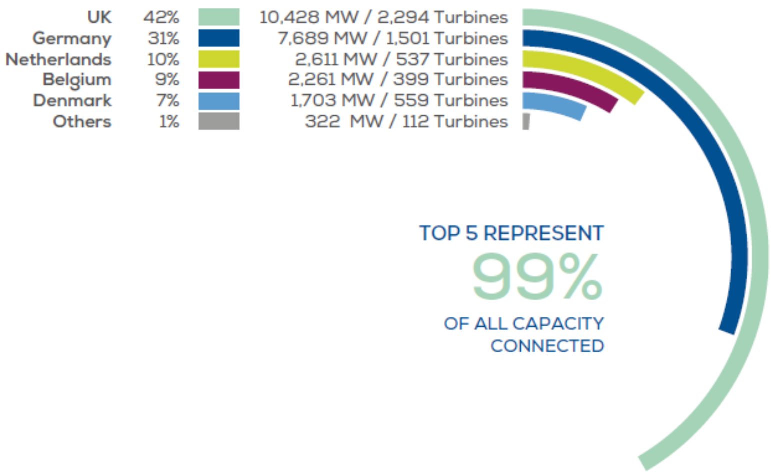


Figure 1.2: The top 5 countries in offshore wind power.[3, p. 14]

Observing Figure 1.3 on the following page it is clear that the power production is moving far from consumption centers as the majority of the WPP capacity is installed in the north sea as mention earlier.

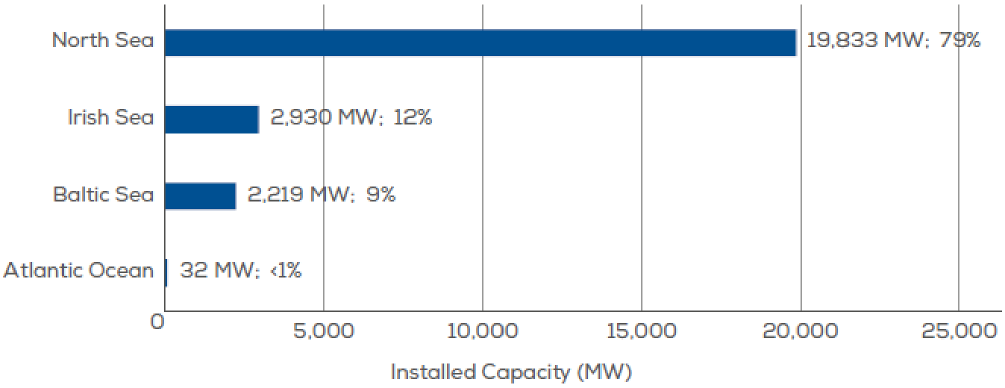


Figure 1.3: offshore wind power capacity at sea.[3, p. 14]

With the development highlighted in Figure 1.2 on the previous page & 1.3 it is clear the penetration of RES specifically from offshore WPPs is expected to increase in the future of the CE power grid. With the increase in offshore WPPs alongside the climate goals of the European parliaments it is expected that the CE power grid is moving towards a power grid with less predictability. The concern in regards to a less predictable power grid is affirmed by the danish TSO Energinet as the power generation of the CE grid is becoming more dependent on local weather forecasts [4, p. 19].

The following section will introduce a historical account of POs through time, and what preventive measures were developed to solve them.

## 1.2 A Brief History of Power Oscillations occurring in Power Systems

Low-frequency electromechanical oscillations in the range of 0.1-2 [Hz] have been observed in power systems since the 1920s, where the earliest forms of oscillations are often referred to as spontaneous oscillations or hunting. This phenomenon (hunting/spontaneous oscillations) was a result of missing damper windings in the generator's prime movers. By adding damper windings that had desirable torque-speed characteristics the occurrence. [5, p. xxiiv]

As power systems worldwide developed further, they were operating closer and closer to their transient and small-signal stability limits. Improvements to the small-signal stability of the power system were made by adding continuous acting voltage regulators to the generators [5, p. xxiv].

In the 1950s and 1960s special care was given to the improvement of the transient stability of the power system. Where the addition of high response exciters to the generators greatly improved the power system transient stability. However, the addition of these high response exciters had had a negative effect on the local plant oscillations with a frequency range of 0.8-2 [HZ] [5, p. xxiv].

This negative effect of the fast-acting exciters increases in severity as power system strength decreases. To combat the negative effect of the fast-acting exciters power system stabilizers (PSS) were developed and deployed in the generator controls to acquire adequate damping of the local mode oscillations [5, p. xxiv].

As the power systems worldwide grew more and more interconnected it gave rise to a new type of oscillation called inter-area oscillations in the range of 0.1-0.8 [Hz]. These oscillations are a product of multiple machines being interconnected through weak tie lines which then form two distinct groups, oscillating against each other during times with heavy power transfer [5, pp. xxiiv-xxiv]. Inter-area oscillations are today becoming a major concern as they can be the root cause for a power system blackout. Traditionally, inter-area oscillation issues have been solved by re-tuning the PSS controls at different generators [5, pp. xxiiv-xxiv].

As mention previously the European power system is expected to see an increase in its penetration of RES in the future thus less predictability as power generation to a greater extend will be dependent on local weather phenomenons. However, the predictability of the power generation is not the only challenge that arises in a power system with a high penetration of RES. This is pointed out by the European member state of Denmark whose TSO, Energinet, points out that with increasing RES the power system will see a decrease in rotating mass thereby a reduction in power system inertia [4, p. 19]. This means the CE power grid will be more prone to power oscillations, as there is less available stored kinetic energy from traditional power plants, that can participate in dampening of power oscillations, in the power system.

From this brief historical overview, it is evident that power systems by nature exhibit oscillatory behavior. And, these oscillations need to be dampened if the power system is to remain in stable operation. Therefore a categorization of these oscillations is needed to distinguish between them.

## 1.3 Categorization of Power System Oscillations

Power system oscillations can be categorized after what components they affect alongside with the frequency range they occur in [5, p. 5].

- Intraplant mode oscillations (2.0-3.0 [Hz]).
- Local plant mode oscillations (1.0 - 2.0 [Hz]).
- Control mode oscillations.
- Torsional modes between rotating plant (10-46 [Hz]).
- inter-area mode oscillations (0.0-1.0 [Hz]).

*** Do note TSOs worldwide may define the range of these oscillations differently***

### 1.3.1 Intraplant mode oscillations

These oscillations occur internally in a power plant site where two or more generators start to oscillation against each other. These oscillations are caused by the generators' different power ratings and reactance. Thus the rest of the power grid is unaffected by these oscillations [5, p. 5].

### 1.3.2 Local plant mode oscillations

Local mode oscillation is where a generator starts to oscillate against the rest of the power grid. This oscillation only affects the generator itself and the tie line connecting it to the system. A solution for removing this type of oscillation is to add a dual input PSS to the generator's AVR [5, pp. 5-6].

### 1.3.3 Control mode oscillations

As the name suggests these type of oscillations is the product of improper tuned exciters, governors, High Voltage Direct Current (HVDC) converters and Static VAR Compensator (SVC) controls. As loads and excitation's system can interact with each through the utilized control. Similarly, tap-changing transformers can interact as they try to keep the voltage within predefined limits, which in turn can lead to voltage oscillations [5, p. 7].

### 1.3.4 Torsional mode oscillations

This oscillation type is related to the turbine generator shaft system. These oscillations can occur if a multi-stage turbine generator is connected to the power grid over a series compensated line. Here an interaction between the mechanical shaft system and the series capacitor occurs at the natural frequency of the electrical system. Where shaft resonance occurs when the natural frequency equals the synchronous frequency subtracted from the torsional frequency [5, p. 7-8].

### 1.3.5 Inter-area mode oscillations

These oscillations arise in large interconnected power systems, where the power grid forms two distinct generator groups, that start to oscillate against each other over a large geographical distance. These oscillations can cause large power swings illustrated in Figure 1.4 over tie lines of the system, which in turn may cause protection relays to trip [5, pp. 6-7].

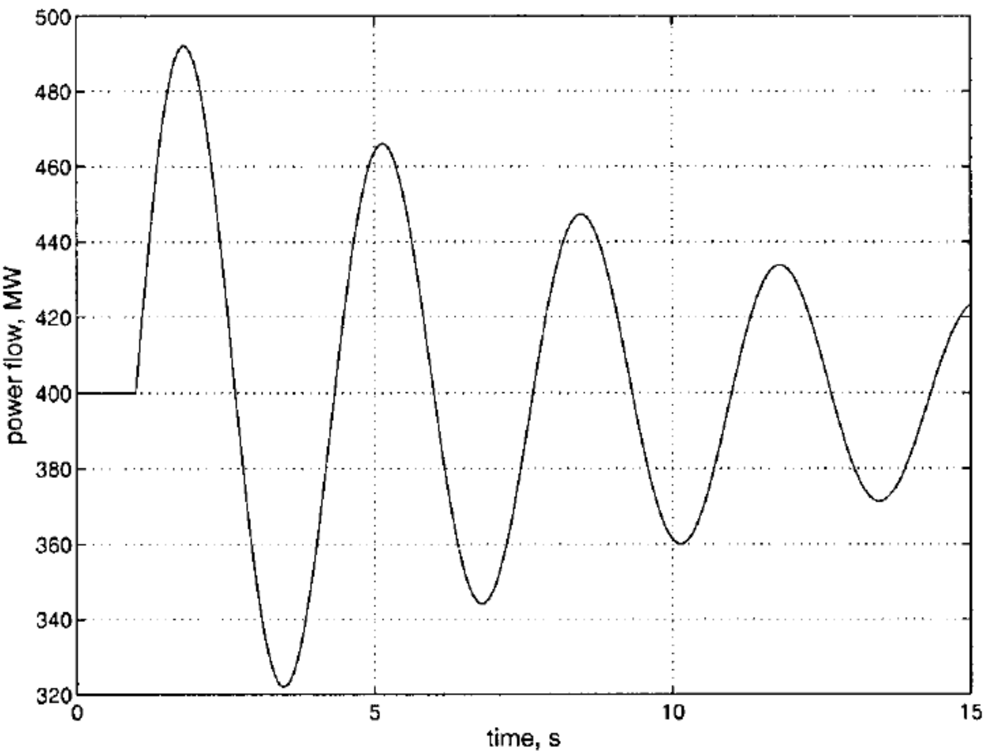


Figure 1.4: Example of how much the power can oscillate during an inter-area oscillation of approximately 0.3 [Hz] [5, p. 7].

Figure 1.4 shows an example of an interarea oscillation causing a power oscillation of approximately 170 MW. This illustrates that operating a power system with only lightly dampened interarea oscillations is difficult as these swings lead to voltage and current variations that may cause protection equipment to react. The reacting of protection relays to the interarea oscillation can lead to power system separation or blackouts [5, pp. 6-8]. Therefore are interarea oscillations a security concern for power systems.

No further explanation of local mode oscillation, intraplant mode oscillation, control mode oscillation, and torsional mode oscillation will be given, as Inter-area POs oscillations are the focus of this project.

## 1.4 Inter-Area Oscillations in the Continental European Power Grid

In this section, an overview of inter-area oscillations observed in the CE interconnected power grid is given. To highlight what preventive measures are utilized to prevent inter-area oscillations from occurring.

The CE synchronous power grid interconnections extend from Greece and the Iberic Peninsula in the south to Denmark and Poland in the north. This interconnected power system is one of the largest in the world and it supplies 450 million customers with an annual power consumption of 2500 [TWh] [6, P. 1]. This also means that the CE power system has multiple AVRs, PSSs and governor systems spread throughout the power system that has to work in collaboration to prevent oscillations [6, P. 1]. As mentioned in subsection 1.3.5 inter-area oscillation can arise as a product of weak interconnected areas. This is also the case for the CE power grid, e.g when there are high winds in the northern region of the CE power grid. Resulting in Denmark exporting excess power to the rest of the CE power grid over the weak tie-line between Denmark and Germany. [6, p. 1].

In [6, p. 4] four main modes of inter-area oscillations have been identified to occurring the CE power grid from [7], which have been cross reference with [8]. And these are illustrated in Figure 1.5

(a) Global mode 1 west east [8]

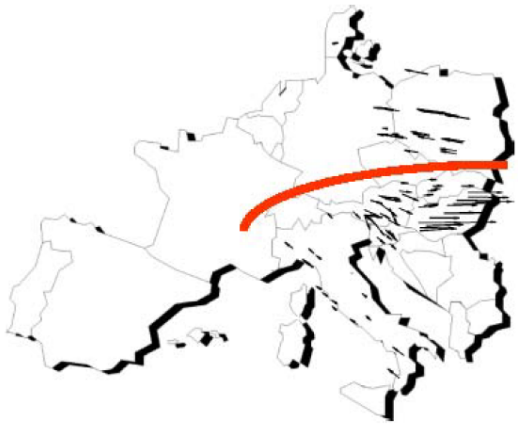

(b) Global mode 2 North south [8]

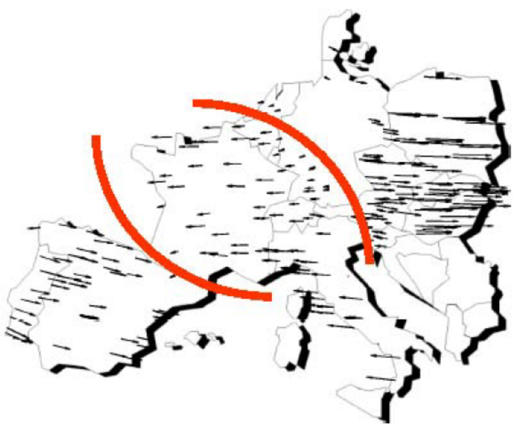

(c) Global mode 3 west east [8]

(d) Global mode 4 north south [8]

Figure 1.5: Illustration of four inter-area oscillation modes observed in CE's power system.

In Figure 1.5 the size of the arrows represents the phasors and the amplitude of the oscillations. Before explaining each mode in greater detail the concept of damping needs to be briefly reviewed.

Traditionally, the damping of electromechanical oscillations has to be damped with 5% or above to be considered adequate. This implies that the initial peak of the oscillation should be damped with 32% after 3 oscillation periods. However, a minimum damping level is unknown, but damping ratios of 3% or should only be accepted with cautions, as too low damping of an oscillation can lead to power system instability. [7, p. 5]

The investigation of how much damping a specific oscillation has is done with eigenvalue analysis. Traditionally the desired damping can be acquired by utilizing one of the three following methods: [6, p. 2]

- PSS acting upon the voltage reference of the AVR in the generator.
- Flexible AC Transmission Systems (FACTS). These devices can control voltage and reactive power quickly to enhance power system dynamic performance.
- Supplementary Control of HVDC links. Done by modulating the current order at the rectifier or current and the voltage. [6, p. 2]

From this list, it is evident that damping of these oscillations is traditionally not done by RES, but with traditional generators, thus as RES penetration is rising this is a topic of concern. The four modes of oscillations are characterized by [6, p. 2-3] as:

- Global mode 1 has a frequency in the range of 0.2 [Hz] and it is the generators of Spain and Portugal, who are oscillating against the generators of the Eastern part of CENTREL. The damping of this oscillation mode is 3.7% and is therefore considered weak.
- Global mode 2 is characterized by a frequency around 0.3 [Hz] and the generators of Spain and Portugal are nearly in phase with generators of eastern Germany and Austria, while in phase opposition to the generators of France, Italy Switzerland, and the western part of Germany and Austria. The damping of this mode is 8.9% thus satisfactory.
- Global mode 3 is characterized by the oscillations occurs at a frequency of approximately 0.5 [Hz]. And it involves the generators of Poland, Hungary, parts of Austria, Slovakia, and Italy. The damping of this mode is not given in [6] thus unknown.
- Global mode 4 is also characterized by a frequency close to 0.5 [Hz]. This mode is not critical for east-west transient but has to be observed in case of bulk power transfer from north to south. The damping of this mode is not given in [6] thus unknown.

By using a Wide Area Measurement Systems (WAMS) several occurrences of inter-area oscillations were detected from 2005-2007 which were not sufficiently damped. Most of these incidents happen doing low load conditions in the power system and mainly involved global mode 1. It is still uncertain what is the cause of these oscillations is, but through re-tuning of PSS controls in both Spain and Greece fewer critical oscillations have been observed. [6, p. 4]

Global mode 4 has been given more attention since it was first observed in 2000, and later confirmed to exist in 2007. This mode involves generators of Denmark, Northern Germany, and the Netherlands oscillating against generators in Italy and Switzerland [6, p. 5]. As this mode of oscillation has low damping it is of concern for system stability. With the increases in offshore wind power plants in the Northern part of Europe, this mode of oscillation is bound to be reoccurring during high winds.

Therefore it is an interesting research topic if RES can provide damping of POs specifically offshore WPPs as the commissioning of off-shore WPPs' are rising in the northern part of the CE power grid. This report seeks to identify if it is possible to acquire a PSS-like functionality implemented as a plant controller in a WPP and if it can perform adequate damping of the oscillation without endangering the stable operation of the WPP.

The next chapter will give an overview of current investigated Power Oscillation Damping (POD) controls performed by WPPs and the gaps in the field in regards to the practical implementation of a POD WPP controller.

# 2 | Project Motivation

This chapter will cover the definition of transient and small-signal stability alongside current grid code requirements for POD from RES in different countries. To highlight the difficulty involved in establishing design criteria for POD from the industry point of view. Lastly, an overview of exiting POD control methods for WPPs is given.

## 2.1 Power system stability

Power system stability refers to a power grid's ability to stay within an operational equilibrium during normal operation conditions i.e. post fault conditions, and its ability to regain stable operation conditions after being exposed to a system disturbance [1, p. 17]. In [1] it is highlighted that the stability problem traditionally referred to the maintain synchronism between the machines of the system. However, this term today can be split into voltage, transient, and small-signal stability alongside midterm and long-term stability, which is illustrated in Figure 2.1.

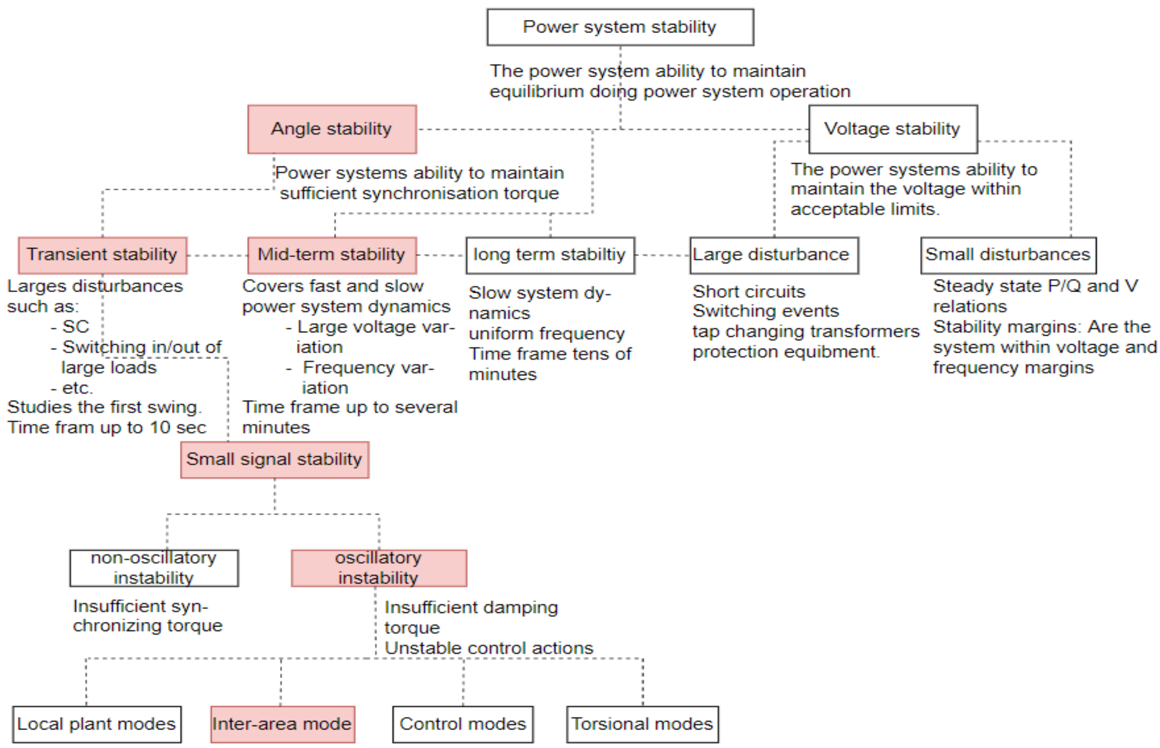


Figure 2.1: Categorization of the stability phenomenon. Inspired by [1, p. 36]

Transient and small-signal stability is defined as:

- Small signal stability refers to small disturbances in the power grid and the ability of the power grid to keep synchronism in the presence of these disturbances. The small disturbances are caused by the dynamic nature of the power system i.e. small variations in generation and load. These disturbances can cause different oscillation modes as described in section 1.3, which means there is a lack of either synchronizing torque causing a steady increase in rotor angle, or lack of sufficient damping torque causing rotor oscillations. [1, p.23]
- Transient stability refers to the power system's ability to remain in synchronism during severe transients. A severe transient can be caused by a short circuit, disconnection of generation, transmission lines, or load. Causing a large power imbalance, which needs to be balanced out with system reserves or control. [1, p.25]

In chapter 1 it was made clear that the area of interest is the inter-area oscillations. These oscillations fall within the angle and small-signal stability category and in turn into the oscillatory instability category, highlighted with a red color in Figure 2.1 on the previous page. Additionally, are the categories, angle stability, transient, mid-term, oscillatory instability, and inter-area mode highlighted in red in Figure 2.1 on the preceding page. These categories are highlighted to illustrate that inter-area oscillations fall into the angle stability category because the inter-area oscillation can last from several seconds to minutes both the transient and mid-term category is highlighted as well to cover the time frame in which the oscillation occurs. The next section will give an overview of exiting grid codes for POD performed by RES from The Netherlands, Ireland, Denmark, and Great Britain.

## 2.2 Grid codes

The exiting grid codes for POD from RES in the countries of The Netherlands, Ireland, Denmark, and Great Britain are shown in Table 2.1. These countries are selected as they are all part of the Northern region of CE and have a large penetration of off-shore WPPs as shown in Figure 1.2 on page 2 & Figure 1.3 on page 3.

| Country | Grid code |
|---|---|
| The Netherlands | If specified by the relevant TSO, Power Park Module (PPM) of type C must be able to provide POD. The implemented controls for the voltage, active and reactive power must not negatively affect the POD. [9, p. 105] |
| Ireland | The grid codes for Controllable PPMs are covered in [10] from page 337-372 covering fault ride through, time frame, frequency ranges for which the controllable PPM must remain connected, active and reactive power control, frequency, ramp rates, automatic voltage control, etc. However, the only mention of POD is in relation to automatic voltage control where it states: *In the event of power oscillations, controllable PPMs shall retain steady-state stability when operating at any operating point of reactive power capability.[10, p. 362]* |
| Denmark | Similarly, to the Irish grid code the danish grid code for WTGs/WPPs in [11] have no requirements for POD, but multiple requirements to voltage, fault ride-through, and frequency. However, Denmark was the first nation in the European Union that invested heavily into wind power on its' west coast. Thus the western part of the Danish power grid (Jylland) operates with a high penetration of RES which can cause the electricity production from WPPs to exceed the power demand in the western part of the Danish power grid which can lead to stability issues. During this development in the Danish power grid, Power Electronic Interface Power Sources (PEIPS) were not developed enough to provide power oscillation damping, and an alternative solution was deployed to solve the power system stability concern. Energinet the danish TSO solved the security concern by enforcing the grid stability with large strategic placed synchronous condenser in the power grid e.g. near HVDC connections. [12, p. 6] |
| Great Britain | Any PPM should provide a range of information ranging from rated power to stator resistance on the generator [13, pp. 52-56] (in section PC.A.5.4). However, the grid code only states under-voltage/reactive power/ power factor control that the plant operator should inform the TSO if a PSS-like functionality is fitted with the associated block diagram [13, p. 57] (in section PC.A.5.4.3.2). There are not given any design requirements in regards to proving the functionality of the PSS control. |

Table 2.1: Grid codes relating to POD from 4 different nations

From Table 2.1 it is evident that it is difficult for the industry to develop and deploy a PSS controller for a WPP as no strict requirements are present from the relevant system operators. This is further emphasized by ENTSO-E which in [12, pp. 5-9] & [14, p. 26] highlights, that research into establishing performances criteria for PEIPS is still an area for research. In [12, p. 7] it is mentioned that even if design criteria were readily available the industry would still need a few years of development before the industry would be able to show that they are compatible with the grid codes. This is further emphasized in [14, p. 7] where it is mentioned that WPP's is already exposed to rigorous certification procedures. In addition to the WTs are expected to have a very high life expectancy. Similar to PV systems if they are to provide POD controls significant development in new hardware and control algorithms are needed before a feasible solution is ready for the market [14, p. 7-8].

## 2.3 Current research on WPP POD controllers

From [12] & [14] and the grid codes in 2.1 on the previous page it is clear that no specific design criteria for POD controls when performed by WPPs is available to the industry. This makes it hard for the industry to start developing product solutions that can perform POD as many RES solutions are exposed to an extensive certification process. Researching the current solutions present in the literature it becomes clear that not much consideration to the practical implementation of WPP plant POD controller is given. Thus this section seeks to highlight these gaps to empathize why a study of a more practical implementation of a WPP POD controller is needed.

In [15] & [16] an aggregated model of a WPP is used, meaning a single DFIG WT is used to represent the entire WPP illustrated in Figure 2.2.

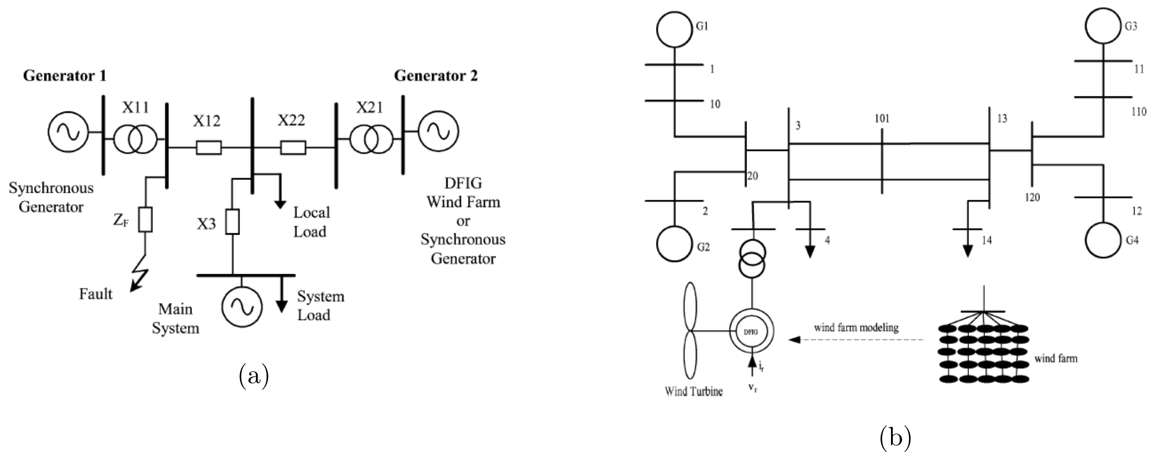


Figure 2.2: Illustration of the test system configuration of (a) [16, p. 1962] & (b) [15, p. 417]

Additionally both articles, ([15] & [16]), utilizes a wound rotor DFIG WT. The operation of the DFIG-WT can be represented by a vector diagram which can be translated into a dq-reference frame. However, here the articles start to differ in their approach as article [16] deploys a Flux Magnitude and Angle Control (FMAC) and [15] deploys a state-space model for the inner control loop of the WT to obtain two PI controllers. The FMAC control aims to enable DFIG WT to provide similar control functions to a traditional SG by controlling the position and magnitude of the rotor flux vector [16, p.1959]. The two PI controllers of [15] translates the current on the q-axis and d-axis to a voltage on the q-axis and d-axis respectively. This control strategy is used to be compliant with the Federal Energy Regulatory Commission order 661 which requires DFIG WTs must be able to control the reactive power from 0.95 lagging to 0.95 leading power factor. By adjusting the amplitude of the voltage vector on the d- and the q-axis respectively it is possible to control the active and reactive power output of the WT thus enabling a vector control scheme. [15, pp. 417-418]

In [16] 3 auxiliary control loops are tested where each auxiliary loop has a different control function. Auxiliary loop 1 enables the DFIG WT to exhibit similar behavior to an SG when observed from the grid side, Auxiliary loop 2 enables the DFIG WT to provide a PSS like functionality to the test grid and auxiliary loop 3 enables frequency support to the grid [16, pp. 1960-1962]. All three functionalities are tested on Figure 2.2a, where all generators and loads are aggravated models, meaning they are equivalent models of a larger generator, load, and WPP. The controls are tested in the system by introducing a fault at t=0.2 s which is cleared after 150 ms [16, p. 1962]. All 3 auxiliary loops are exposed to this fault in order to evaluate their performance from which the authors conclude the following [16, p. 1965]:

1. FMAC control can emulate SG behavior if AUX loop 1 is utilized.
2. FMAC control can provide PSS function if AUX loop 2 is utilized and dampens POs.
3. FMAC control can provide frequency support in case of loss of generation if AUX loop 3 is utilized.

In [16] it is not considered how to practically implement any of the 3 auxiliary control loops in a WPP controller. Indicating that not much consideration to if the FMAC control reflects the behavior of overall plant control, or if this control structure is needed at every WT in the WPP, where the WPP controller then only generates the stability signal for all the WTs. Additionally, the acquisition of measurement signal at the point of connection (POC) has not been modeled, which indicates the controls in [16] does not consider any measurement delay, computation delay, or the resolution of the measurements.

In [15] the open-loop response of the system is plotted in a root locus diagram. From the root locus diagram, the authors of [15] observe that the order of the model is too high. Therefore an approximation of the open-loop system is made by using the dominant poles and zeros of the system to construct a transfer function. The transfer function of the open-loop system is then utilized to design a POD control. [15, p. 419]

In [15] similarly to [16] modeling of measurement devices to acquire the needed input to the control is not considered [15, p. 418], As [15] also uses an aggregated model of a WT it is not clear if each WT should be equipped with the developed control scheme or if the control scheme is the WPP controller. Additionally in [15] the frequency for the inter-area oscillation is known, therefore it is possible to design the controller specifically to dampen the inter-area oscillation present in the power system. Thereby the controller has not been exposed to a range of inter-area oscillations, where it may not perform as intended. Thus it could be argued that not much concern regarding filtering is given to ensure the control only reacts to inter-area oscillations. It was investigated in [17] how a PMSG-WT can contribute to the system inertial response and if it can provide POD. The PMSG-WT utilized is a variable speed turbine which means the rotor speed of the turbine is independent of the grid frequency. Therefore can a PMSG-WT have a virtual inertia value several times higher than its' natural inertia as the rotor can have an angular speed that is greater than the grid frequency. This also means the PMSG-WT virtual inertia as seen from the grid is strongly dependent on the weather conditions, as higher wind speed would result in a higher rotor speed of the turbine, which in turn results in an accumulation of more kinetic energy stored in the rotor. Where for comparison a traditional SG has a fixed rotor speed which is synchronously coupled to the power systems grid frequency. [17, pp. 566-567] The design of the virtual inertia controller is based around the method: Optimized Power Point Tracking (OPPT). The reader is referred to pages 567-569 of [17] for a detailed explanation of the control. The controller is tested in the laboratory on a 3 bus system illustrated in Figure 2.3. In the illustrated test system the RES penetration is around 31%. The sampling time for the control system is 50 $\mu$s and the PWM frequency of the PMSG converters is 10 kHz. Gen1 participates in frequency regulation as it is equipped with a 4% droop control where Gen 2 is operating in constant active power mode. The power system is exposed to a 3-phase short circuit (SC) fault lasting 0.1 s to initialize a power swing. From the test results, it is concluded that the proposed OPPT control scheme enables the PMSG-WT to contributed power oscillation damping [17, pp. 570-573].

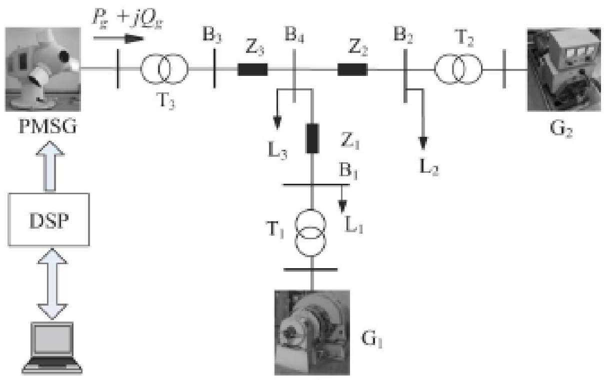


Figure 2.3: Illustration of the test setup in [17, p. 570]

Like in [15] & [16] the utilized model is a 3 area system, with only a single turbine modulated to provide the OPPT control scheme, which means the control scheme proves that POD can be performed by a single turbine, but not how to implement it in a WPP controller. Similarly, the data acquisition is done by a DL850, CRIO-9025 controller, and NI data acquisition cards, indicating that no modeling of actual power grid measurement equipment is done. Lastly, it has to be mentioned that the utilized sampling time of 50 $\mu s$ is unrealistic, as in [18, p. 25] it is mentioned that a time delay of 15 ms is typical to use for the acquisition of measurements at the PCC. Which is further affirmed by the grid meter manufacturer Bachmann e.g. their GSP274, GN260, GMP232/X, acquire the phasor measurements at an interval of 10 ms, 10 ms, and 3.3 ms true RMS respectively [19]. Indicating that the time delay introduced by the phasor measurement alone is greater than the overall deployed time delay in [17]. All three articles [15], [16] & [17] do not consider if the internal angle of separation between the individual WTs can affect the proposed control schemes. The internal angle of separation that arises from WPPs covers a larger geographical area, resulting in that each WT sees a different impedance to the PCC. In [20] this issue is investigated and analyzed to see if a WPP can participate in POD or if the angular separations between the WTs are too high preventing the WPP from having a uniform response at the PCC [20, p. 431]. The analysis is done upon a 5 area system illustrated in Figure 2.4 where the WPP at the POC contains 150 WTs. The WTs are a model of a 3.6 MW Siemens Wind Power WT that includes a variable wind speed aerodynamic model, a two-mass model of the rotor, gearbox, and generator, machine and grid side converter[20, p. 433]. The authors investigate what oscillations are present in the power grid through modal analysis, where it is identified from the eigenvalues of the system that there are two poorly damped inter-area oscillations of 0.54 and 0.41 Hz present in the grid [20, p. 434].

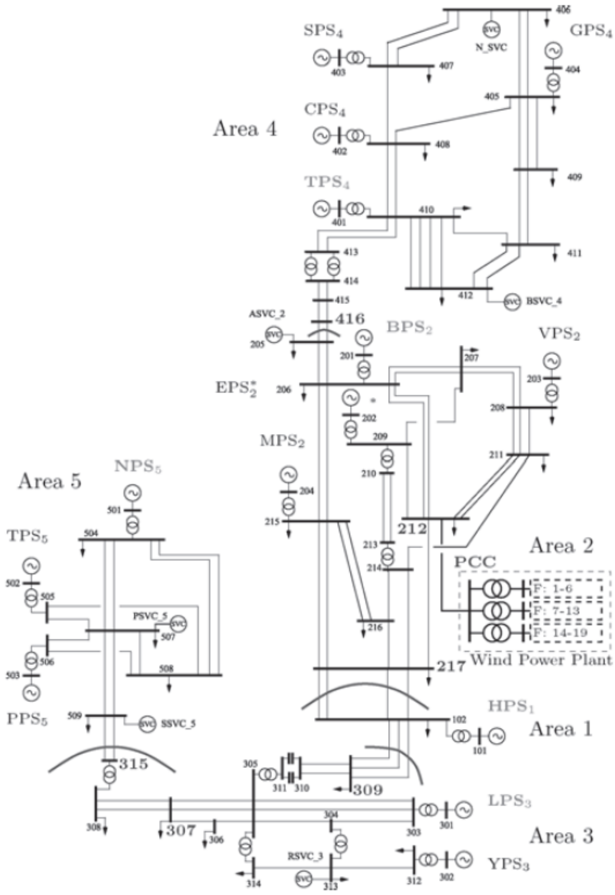


Figure 2.4: Illustration of the system size used in [20, p. 433]

It is investigated if the magnitude and angle for active and reactive power modulation residues are too big indicating if the angular separation between the WTs is too big for the WPP to provide POD. For the active power modulation, it is found that the angle residue of the active power is in the range of 0.5° to less than 3.0° where the reactive power modulation residue ranges from 5° to a maximum of 14°. [20, p. 435]

From this analysis the authors test a POD WPP control utilizing $\Delta P$ or $\Delta Q$ which utilizes local measurements to compute the stabilizing signal forwarded to the individual WTs. The $\Delta P$ POD directly affects the active power reference of the WT where the $\Delta Q$ POD affects the WT voltage reference to control the reactive power output of the turbine. The POD control is handled by the following transfer function:

$$G_{POD} = K\frac{sT_{wo}}{sT_{wo}+1}\frac{1}{sT_{lp}+1}G_{pc}(s)$$

Here K is the gain, $T_{wo}$ is the washout filter constant, $T_{lo}$ is lowpass filter constant and $G_{pc}(s)$ is the transfer function for the phase compensation. The system is then exposed to a 3-phase SC lasting for 50 ms at bus 307 in area 3.[20, p. 435] From this investigation the authors concluded that both the active and reactive power modulation the angular difference between the individual turbines are small enough for a WPP POD controller to be used. However, they also conclude that additional work is required to ensure that the WPP POD controls does not interfere wiith WTs fault ride through.[20, p. 441]

In [20] modal analysis has been performed which involves the computation of the system's eigenvalues. Indicating that the utilized model is modeled in great detail to capture the present POs and design a control scheme to dampen them. This is impractical as it would require the industry to have a detailed model available of the CE power grid in Europe to develop, and tune their WPP controller after. Another issue to this is when the grid undergoes changes from either maintenance or upgrading of equipment the dynamics on the power grid change, meaning the developed and tuned WPP controller may now be ill-suited to perform POD.

Multiple solutions for how to perform and develop a POD controller for a WPP have been reviewed illustrating there are multiple approaches to the topic. This is further confirmed by [21] where multiple solutions to POD performed by WPPs are reviewed and if the solution helps with improving system stability.

Additionally in [21] it is pointed out that the basis for small signal stability is a mathematical model of the power system where it is represented by a set of nonlinear differential equations and algebraic equations which can be translated into a state-space representation of the power system. If this model of the system is linearized around a working point it enables eigenvalue analysis which in turn can identify the different oscillations and asses if they are sufficiently damped or not. Lastly, it is mentioned that most of the research done in literature utilizes an aggregated model of WPPs. [21, 4996]

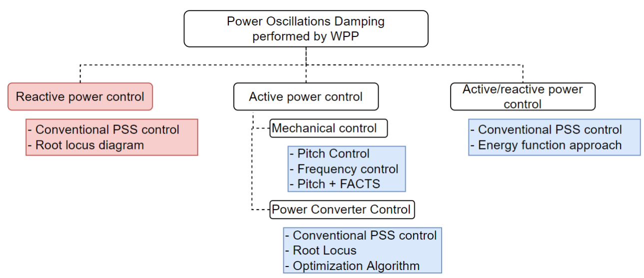


Figure 2.5: Block diagram representation of the different solutions from literature. Inspired by [21, p. 5003]

Additionally [21] highlights that special care must be taken in regards to the inner oscillations of WPPs as these can have detrimental consequences for the lifetime of the WPP installations if these are not damped. available options for damping of these oscillations range from PID torque controller to dampen torsional oscillations, a conventional PSS scheme that controls the DC link by utilizing the machine speed as an input, pitch system control among others [21, pp. 4998-4999].

From the litterature it becomes evident that there are multiple options for performing POD control, this is illustrated in Figure 2.5 on the preceding page. These option range from mechanical to converter controls and from active to reactive power control or a combination of the two. Note the the reactive power control option is highlighted in red because the proposed controller in this report will operate in this category, and the reason for this decision will be explained later in the report. A summary of the found gap from literature in regards to the practical implementation of a WPP control is given in the following table:

| Sources | Model size | Modeled consideration | Model drawbacks | Ability to dampen POs |
|---|---|---|---|---|
| [15] | 3-area system | - DFIG WTG wound rotor<br>- dq-reference frame<br>- state space model<br>- compliant with grid code order 661 | - Aggregated models of: WPP Generators loads<br>- No consideration for PCC location<br>- Time delays<br>- Single WT control or WPP control<br>- No modeling of grid meters | Yes |
| [16] | 3-area system | - DFIG WTG wound rotor<br>- dq-reference frame<br>- FMAC control scheme<br>- 3 Auxiliary control loops | - Aggregated models of: WPP Generators loads<br>- No consideration for PCC location<br>- Time delays<br>- Single WT control or WPP control<br>- No modeling of grid meters | Yes |
| [17] | 3-area system | - RES penetration 31%<br>- Variable speed drive<br>- Virtual inertia control<br>- small scale<br>- Laboratory setup with data acquisition | - Unrealistic sampling and switching frequency<br>- No modeling of grid meters<br>- Single WT control<br>- Small laboratory setup. power level and data acquisition does not represent a grid situation | Yes |
| [20] | 5-area system. | - No Aggregate models<br>- WPP models 150 WTs<br>- Modal analysis<br>- Active/ reactive power modulation<br>- WPP controller<br>- Angular separation between WTs considered<br>- Location of PCC | - Practicality of modal analysis as it requires great system knowledge which may unavailable to the industry<br>- No modeling of grid meters<br>- Time delays | Yes |
| [21] | - | - | - | Review of multiple solutions to dampen inner WT oscillations as well as solutions for WPP POD controllers. |

Table 2.2: Model consideration and drawbacks from literature study.

# 3 | Problem Statement

With the drawbacks from literature highlighted in Chapter 2 in Table 2.2 on the previous page. This chapter will outline main and sub-objectives to be solved in this study,alongside with the relevant delimitation.

From Chapter 1 it is pointed out that the CE power system is seeing an increase in commissioned WPPs in the Northern region. This gives rise to a new set of challenges such as how WPPs should participate in POD. Multiple solutions are present in literature, for which a brief overview was given in Chapter 2. Many of these studies utilize aggregated models of WPP, thereby representing the entire WPP by a single WT implying this is a suitable approach to test POD controllers' performance for an initial design. However, not much concern is shown to exiting grid codes and the constraints they will introduce to the deployed control scheme. With these issues presented the main objective and sub-objectives can be formulated as:

***How to define a set of practical design criteria for an implementation of a WPP POD controller. Accounting for grid codes, time delays, and controller action.***

**Sub-objectives**

1. *Investigate available measurement devices from the industry in regards to their introduced time delay*
2. *Analyse state of the art filtering solutions in order to enable the WPP POD controller to perform POD at multiple frequencies without endangering the operation of the individual WTs.*
3. *Do the developed WPP controller provide sufficient damping of the investigated PO frequencies.*

## 3.1 Delimitation

The delimitations of the study is given in the following list.

1. *The project does only take the Danish grid codes into account during the development of the POD controller.*
2. *The study will only focus on WPPs in the D power class from the Danish grid codes.*
3. *The controller is developed for a 50 Hz network.*
4. *The only voltage level considered is 400 kV.*
5. *The study utilizes an aggregated model of a WPP, and it is not investigated how the controller affects the internal configuration of a WPP.*
6. *The aggregated WPP model is based upon the danish WPP Horns Rev 2, meaning no considerations have been given to other WPPs' power levels.*
7. *The study do not utilize eigenvalue analysis to identify PO's, but assumes they can be identified from grid meter measurement at the PCC.*
8. *The on-shore power grid is represented as a voltage source behind an equivalent impedance estimated from the grid SCR and XR ratio.*
9. *The internal transmission path of the WPP is not modeled, implying that the developed POD controller has not accounted for internal phase shift and angle of separation caused by the internal transmission path.*
10. *The study does not consider the eigenfrequencies of the WTGs, thereby can the POD controller act in the entire inter-are frequency range.*
11. *The study does only consider a PSS-like control option based upon a traditional PSS controller for an SG. All other control options are considered to be outside the scope of the project and have not been investigated further.*
12. *The proposed POD controller is to act on the reactive power reference of the WPP, and no investigation is done in regards to active power control*

## 3.2 Methodology

To highlight the concerns on the area of inter-area oscillations a literature study is performed. The literature study covers the extent of detected inter-area oscillations present in the CE power grid, and a study of proposed methodologies for performing POD with a WPP. The POD WPP control aspect of the literature study is analyzed concerning a practical implementation of the control. E.g. would detailed power system information be available to the industry, etc. The design and tuning of the WPP POD controller will be done with the aid of Mathworks Matlab and Simulink to analyze the performance and stability of the initial design.

# 4 | WPP architecture and design considerations

This chapter will describe the different elements in the drawing illustrated in Figure 4.1. The chapter will also explain the proposed control topology, and the design considerations considered in this report.

## 4.1 WPP architecture

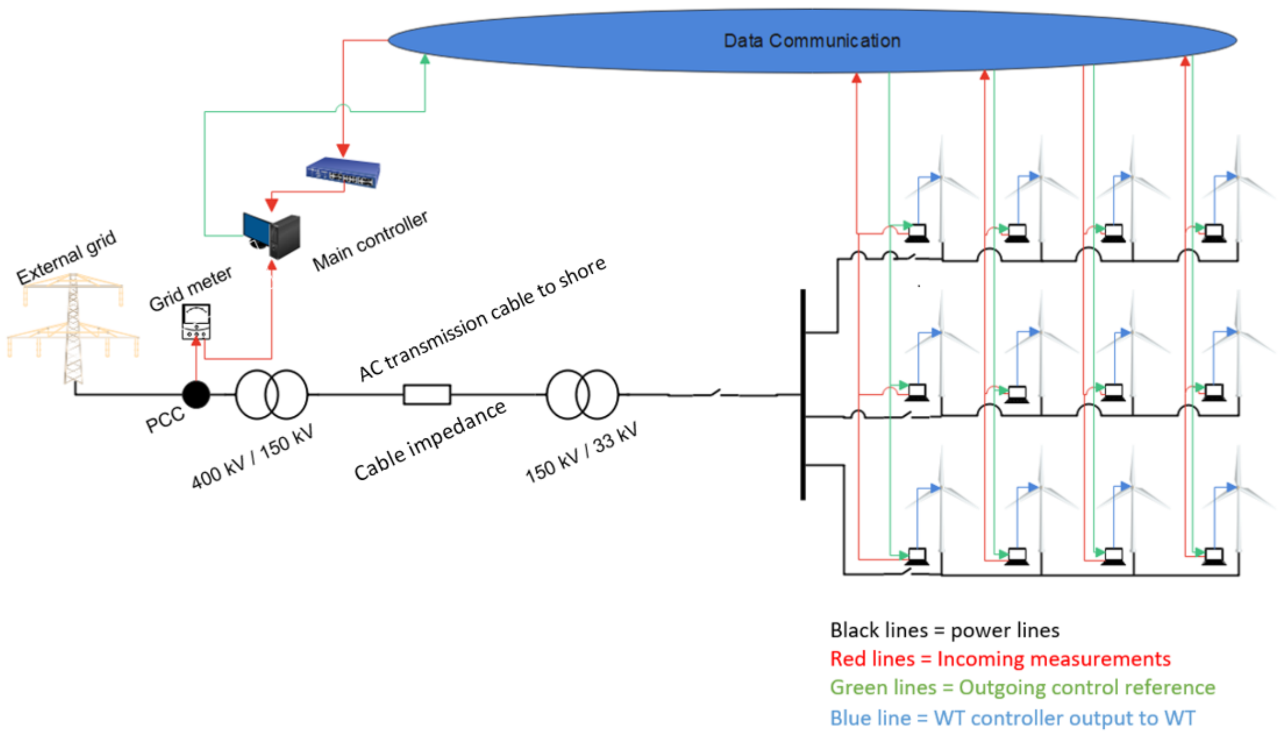


Figure 4.1: Illustration of a WPP arcitecture.

In Figure 4.1 an illustration of a WPP is shown. However, in reality, WPPs contain more WTs than the 12 shown in the Figure. E.g. Horns Rev 1, 2, and 3 on the west coast of Denmark contains 80, 91, and 49 WTs of size 2.0 MW, 2.3 MW, and 8.3 MW respectively. The rated active power of Horns Rev 1, 2, and 3 are 160 MW, 209 MW, and 406 MW [22]. The rated power output of the WPP depends on utilized WTs in the park. For this project Horns Rev 2 is arbitrarily chosen as a baseline and it is assumed that Horns Rev 2 rated reactive power is equivalent to its rated active power, thus $Q_{rated}$ = 209 MVAr. Lastly, it is also assumed that the WPP cannot deliver full rated active power and reactive power simultaneously.

This also means that the power transformer connecting the WPP to the grid both at the offshore substation and at the onshore substation must at a minimum be rated at 209 MVAr. Observing Figure 4.1 on the preceding page it is clear that there are multiple voltage levels present. The internal grid voltage of the WPP is 33 kV which is based upon Horns rev 1 and Horns rev 2 [23] [24]. The power from each WT is fed into a feeder which is then connected to the offshore substation with the first transformer, which increases the voltage from 33 kV to 150 kV and transmits the power to shore. The distance between the WPP and the shore varies depending on the WPP location e.g. Horns Rev 1 is located 21 km off-shore where Horns Rev 2 is located 42 km off-shore. When the power arrives at the onshore transformer substation the voltage is increased from 150 kV to 400 kV AC to transmit the power from WPP to where it is needed in the power grid. [23] [24]. From the transmission path illustrated in Figure 4.1 on the previous page the nominal park voltage is assumed to be 33 kV and the nominal power grid voltage is assumed to be 400 kV.

However, as mentioned in the project delimitations the internal transmission path of the WPP is neglected, and the WPP is modeled as being directly connected at the PCC. Additionally only the 400 kV voltage level is model, meaning the WPP operates at this level as well.

The layout, voltage level, and power level of the WPP shown in Figure 4.1 is based upon Horns rev 1 through 3 which all are located on the west coast of Denmark. In reality the size, voltage level, and power ratings will depend on where it is located in the world e.g [25, p. 1] a different architecture is used. Here the nominal voltage level of the internal grid of the WPP is 34 kV, the offshore substation increases the voltage to 150 kV, and the onshore substation increases the voltage to 275 kV to transmit the power from the WPP to where it is needed in the power grid.

From Figure 4.1 on the preceding page it is seen that a WPP is a layout consist of a number of parallel strings of WTs. In each string, the WTs need to be appropriately spaced from one another to maximize power production from the WTs. As the wind passes the WT it extracts energy from the wind as it passes the turbine causing turbulence in the airflow. This in turn reduces the wind speed, thus the energy content in the wind, therefore, should the WTs be at least spaced 3 rotor diameters from one another to reduce the wake effect. [26]

Additionally, it has to be mentioned that there is a limit to how many WTs can be put in a string. This is dependent upon the power rating of the WTs as it will decide the maximum current they can deliver to the feeder. For E.g. Horns Rev 2 consists of 7 turbines in each string resulting in 13 parallel strings accounting for the 91 WTs in the WPP. If the WPP produces its rated power at unity power factor that would result in a load current of 484.87 A per string. If all of the strings are fed to the same feeder that would result in a current of 6.34 kA. Illustrating that there is a limit to the number of

WTs that can be put in a string as the load current will increase putting more strain on power system components. With an increasing current, the different elements in the transmission path of the power system need to be appropriately chosen to keep power losses at a minimum when transmitting bulk power [27, p. 17].

The coming sections will explain the various elements of Figure 4.1 on page 22 starting with the WTs.

## 4.2 Wind Turbines

In this study it is assumed that the WTs are type 4 turbines, meaning they are variable speed turbines interfaced to the power grid over fully rated power converter. This means the generator of the turbine is completely decoupled from the power grid as illustrated in Figure 4.2.

Having the WT completely decoupled from the power grid enables flexibility as the turbine generator does not have to rotate at the grid frequency. Thereby can the WT generator rotate at the most aerodynamic speed optimizing the power delivered by the WT, but it does also create what is called a wild AC output [28, pp. 20-21].

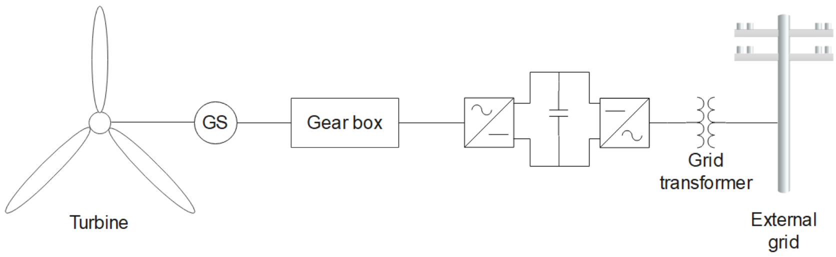


Figure 4.2: Illustration of a type 4 turbine. Inspired by [28, p. 21]

The fully rated converter can provide an additional benefit as it enables the internal control loops for active and reactive power to be decoupled from each other. thereby can the converter of WT control the amount of active to reactive power injected into the power grid. [21, p.5002] [29, pp. 290-292]

The WPP plant controller then controls the reference given to each WTG power converter thereby adjusting the power injected into the power grid.

In the next section considerations concerning the modeling of the external grid illustrated in Figure 4.1 on page 22 is explained

## 4.3 The External Grid

The external grid of Figure 4.1 on page 22 can be approximated as a Thevinen equivalent as illustrated in Figure 4.3. Here the grid voltage is modeled as a voltage source behind an impedance. This is a simplification of the actual external grid, but it is accurate enough for load flow analysis and RMS simulations containing inter-area oscillations [30, pp.47-50]. The magnitude of $Z_G$, $R_G$, and $X_G$ can be found by the Short Circuit Ratio (SCR) and the XR-ratio of the grid. The SCR ratio at a point in the grid is computed as the SC power ($S_k$) at the point divided by the rated power of the power plant supplying power to the specified point described in eq. 4.1

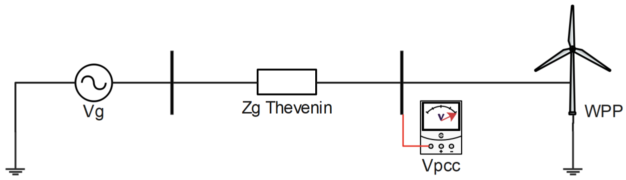


Figure 4.3: Illustration of the Thevenin approach.

$$SCR = \frac{S_k}{P_{rated}} \tag{4.1}$$

Where the XR-ratio describes the amount of reactance that goes to the amount of resistance present in the network and it is calculated as described by Equation 4.2

$$XR\text{-}ratio = \frac{X}{R} \tag{4.2}$$

From the SCR and XR-ratio the magnitude of the grid impedance, resistance and reactance can be estimated by eq. 4.3 through 4.5.

$$Z_g = \frac{V_g^2}{S_k} \tag{4.3}$$

$$X_g = Z_g \cdot \sin(\tan(XR)^{-1}) \tag{4.4}$$

$$R_g = Z_g \cdot \cos(\tan(XR)^{-1}) \tag{4.5}$$

The SCR value provides information about the grid stiffness at the PCC. A high SCR value implies a low grid impedance resulting in a small voltage drop between the external grid and the PCC [18, p.12]. The grid is considered to be stiff if the SCR is above 20 (SCR>20) at the PCC [30, p.50]. Similarly, a common value for the XR-ratio is 10 [30, p. 50]. In the coming section, the internal communication between the WPP and the WPP controller will be examined and explained.

## 4.4 Data communication

There are multiple communication lines illustrated in Figure 4.1 on page 22 highlighting the internal flow of data between the WPP controller and the individual WTs. The lines do not represent individual communication cables. In practice, all of the communication will be carried by a single cable. The red lines are incoming information from the measurement at the PCC and the individual WTs delivered to the WPP plant controller. The WPP plant controller processes this data to determine the new power reference for the WPP then the controller forwards the signal to the WTs illustrated by the green lines. The WT controller receives the new reference and adjusts the power output of WT, illustrated by the blue line.

### 4.4.1 Data acquisition at the PCC

Data acquisition at the PCC is performed by a grid meter, for which multiple hardware solutions are available on the market, but common for all of them are they all introduce a time delay. In [18, p. 25] it is mentioned that a typical time delay for the acquisition of data from the PCC is 15 ms. Investigating various grid meter solutions from [19], [31] and [32] it is found that they introduce a time delay of 3.3 ms to 20 ms depending on the chosen hardware solution. Therefore is an average time delay of 10 ms chosen to represent the grid meter at the PCC.

### 4.4.2 Approximation of communication delays between WPP plant controller and WTs

The authors of [33] propose a new communication architecture called smart WPP communication. This architecture aims to improve the communication between the WTs and the plant controller to maximize the power output of the WPP [33, p. 3900]. The [33] article helps establish the baseline for the communication time delay between the WTs and the WPP controller. Additionally, it will also be used to establish the internal time delay in each WT.

The internal time delay in the WTs is approximated to be 4 ms in article [33]. This time delay covers the acquisition of the measurement, treatment of measured data, and/or treatment of the new reference given by the WPP controller to the WT which then adjusts its power output accordingly [33, p. 3919]. The time delay of 4 ms does not cover the communication delay between the individual WTs and the WPP controller.

The communication in the WPP is assumed to be a single EPON cable connecting an entire string of WTs in each row. Even though a parallel configuration of EPON cables would increase the reliability of the communication it will also significantly increase the number of EPON cables used thereby increasing the cost of the WPP [33, pp. 3914-3915]. Thus the cheaper solution is adopted for this study.

Because the communication takes place over a single EPON cable per string of WTs, the communication is executed in a hop-by-hop manner. This implies the communication of the new reference from the main WPP controller is given to one WT at a time. When WT controller acknowledges it has received the new reference the signal will hop by to the next WT [33, p.3913]. This communication architecture introduces a time delay from WT to WT which has to be approximated. The authors of [33] investigated how the transmission of weather forecasting data is affected by the utilized hardware for a single standalone WT. From this investigation, they found that the introduced time delay between the single WT and the controller where 13.88 ms for a EPON link with a speed of 100 Mbps. Where if a 1 Gbps link is used it reduces the time delay from 13.88 ms to 0.073 ms. This indicates that the introduced time delay from communication between the WPP main controller and the individual WT is strongly dependent on the installed hardware as well as the amount of data transmitted [33, p 3919].

The communication delay between the individual WTs is approximated to be between 0.073 ms to 13.88 ms based upon the findings in [33]. Because the distance between the WTs is typically short (500-600 m [23],[24]) the communication delay between each WT is approximated to be 5 ms. It has to be emphasized that the delay of 5 ms is an approximation as no information about the communication hardware utilized in either [23] and [24] is known. Thus the time delay of a string containing 9 WTs is illustrated in Figure 4.4

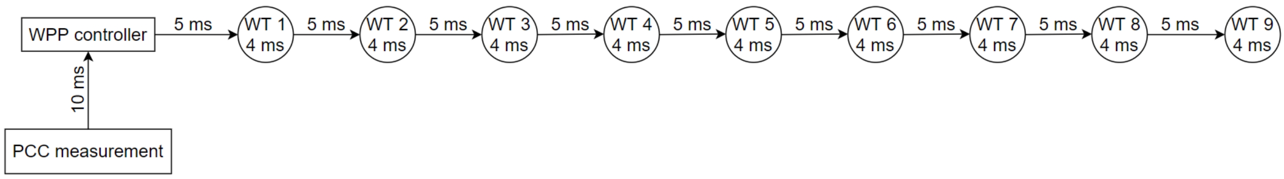


Figure 4.4: Illustration of communication delay

The combined time delay of each component PCC measurement, communication delay, and internal WT delay is then added up and given in Table 4.1.

| Component | Individual delay | Combined delay |
|---|---|---|
| WT | 4 ms | $9 \cdot 4 = 36$ ms |
| PCC measurement | - | 10 ms |
| Communication delay | 5 ms | $9 \cdot 5 = 45$ ms |
| Total time delay | - | 91 ms |

Table 4.1: Overview of the time delays from acquisition of data at PCC, per WT and communication between each WT of a single string in the WPP

The total time delay of Table 4.1 will be implemented in the simulation environment as the time that passes before the WPP POD controller starts acting upon the PO. Lastly, the authors of [33] also investigated a wireless communication option. However, a communication configuration of this structure appears to still be in the research phase and not used by the industry therefore it is not considered in this study.

Having established the time delays for the WPP the danish grid code for WPPs is investigated to establish what design considerations are relevant for the proposed POD controller in the coming section.

## 4.5 Considerations for POD controller requirements at the PCC

Even though the danish grid code for WPPs ([11]) has no specific requirements for WPP POD controllers it is still reviewed to identify what constraints the POD controller have to be compatible with. In [11] there are 4 different power classes for WPPs, each having different requirements to available control functions. These categories are listed in Table 4.2.

| Category | Power range |
|---|---|
| A2 | From 11 kW to and including 50 kW |
| B | From 50 kW to and including 1.5 MW |
| C | From 1.5 MW to and including 25 MW |
| D | Above 25 MW or connected at 100 kV |

Table 4.2: WPP categories and their respective power ratings [11, p. 30]

Investigating the power ratings of Horns Rev 1,2 and 3, which are 160 MW, 209 MW, and 406 MW respectively, it is evident that all 3 WPPs are in the D category of Table 4.2.

A WPP in the D category is required to have the following control function available and be able to control its power output at the PCC [11, p. 47-48]:

- Frequency response (FR)
- Frequency control* (FC)
- Absolute Power constraint (APC)
- Delta power constraint (DPC)
- Ramp rate constraint (RRC)
- Q control* (QC)
- Power factor control* (PFC)
- Voltage control* (VC)
- System protection

The star (*) indicates that if the plant is to perform this control, an agreement with the TSO must be established before the control can be deployed. The system protection aspect will not be investigated in this study.

It is evident from the list of control options that the POD controller cannot be compatible with all of the restrictions in each category of control given in the danish grid codes [11]. As each control type has different requirements thus a category will be selected that the POD controller must be compatible with.

The POD controller is selected to act upon reactive power, and therefore it should be compatible with the restrictions present for QC, PFC, and VC control, in addition, to be compatible with the ramp rate constraint for reactive power. The reason for making the POD controller compatible with the restrictions in reactive power control is because there is more room for control action. The room for control action comes from the allowed ramp rate for reactive power is 10 MVAr/s, which is 100 times bigger than the allowed ramp rate for active power of 100 kW/s thereby enabling a quicker controller. Depending on which area the POD controller is implemented as an additional auxiliary control the time frame varies. For QC and PFC a control action has to start within 2 seconds upon the receipt of the control signal and complete the control action within 30 seconds. Where if the POD controller is to act upon the voltage it has to start the control action within 2 s upon receipt of the new reference and complete it within 10 s. The last constraint introduced by QC, PFC, and VC is that $Q_n$ is not allowed to vary with more than 2% over a minute after a complete control action. [11, pp. 49-56]

Lastly, the danish grid code for CHP plants given in [34] has to be considered because it is in this grid code the danish TSO defines the range of frequencies which they consider to be inter-area oscillations. The Danish TSO defines inter-area oscillations to be within the frequency range of 0.2-0.7 Hz. As the aim of the POD controller is to fulfill the same role as a traditional PSS controller it should be held to the same standard. Thus, the developed POD controller must not adversely affect the damping of local oscillations [34, p. 47] similarly to the PSS controller installed on a traditional generator. This also implies that the WPP POD controller should only act within the defined inter-area frequency range. As the WPP POD controller will adopt a PSS-like structure of a traditional PSS control utilized in SGs, its structure will be explained in the following section.

## 4.6 Traditional PSS controller

In Figure 2.5 on page 17 it is shown that a conventional PSS can perform POD in a WPP setting. Thus, an illustration of the block diagram of a traditional PSS is shown in Figure 4.5.

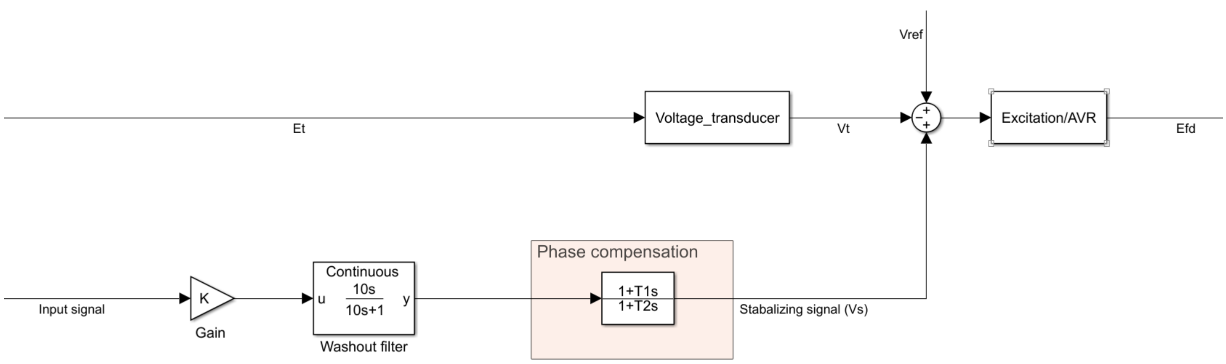


Figure 4.5: PSS block diagram, inspired by [1, p. 769]

It is observed in Figure 4.5 that the PSS controller can be implemented as an additional input to the SG excitation system to enhance small signal stability [1, p. 335]. When adding additional control to the power system care must be shown such that the addition of the PSS enhances the overall system stability [1, p. 770]. The addition of a PSS enhances the small-signal stability of the system by dampening unwanted rotor oscillations/POs thereby it enhances the overall system stability if tuned correctly [1, p. 767]. The POs can arise from various causes, such as load changes, contingencies, or excess power production.

Common inputs for the PSS is shaft speed $\omega_r$, terminal frequency $f_e$ and power $P_e$ [1, p. 335]. With one of these inputs, the PSS translates it to the stability signal $V_s$ which is then summarized with the terminal voltage $V_t$ and the voltage reference $V_{ref}$ and then forwarded to the excitation/AVR system. Thus the PSS achieves dampening of the unwanted rotor oscillations by providing an electrical torque component ($T_e$) which is in phase with the rotor speed deviation counteracting the rotor oscillation [1, p. 766].

The PSS is comprised of a gain block, washout filter, and a phase compensation system, and the purpose of each block is explained as follows:

1. **Gain block** determines the amount of damping provided at a certain frequency [1, p. 770].
2. **Washout filter** prevents steady signal changes to pass through and affects the excitation voltage reference. And has the transfer function:

$$Washout\ filter = \frac{T_w \cdot s}{T_w \cdot s + 1} \tag{4.6}$$

   The time constant $T_w$ is considered a noncritical parameter, however, it is tuned after what area the PSS should provide damping in. E.g. if the PSS shall provide dampening of local area oscillations an appropriate value for $T_w$ is in the range of 0.8-1.5, where if the PSS is to provide dampening of inter-area oscillations an appropriate value for $T_w$ is 10 or above. [1, pp. 1133-1334]
3. **Phase compensation system** traditionally has a phase lead characteristic as it has compensated for the phase lag between excitation input and the electrical torque component of the SG [1, p. 769]. The phase compensation system is typically tuned to be slightly uncompensated with up to 10° to prevent the PSS from introducing negative synchronizing toque component [1, p. 1133].

### 4.6.1 Application of PSS for WPP controller

The WPP controller controls the output of the WPP by adjusting the reactive power reference given to the WTs of the WPP. The time constant $T_w$ is set to 10 as it is an appropriate value when dampening of inter-area harmonics is wanted. In a traditional PSS, a single lead-lag block is sufficient in compensating for the lag introduced by the SG excitation system, however, the phase compensation system in the WPP controller has no excitation system. Meaning the damping signal must be in anti-phase with the original signal to achieve dampening. Thus multiple lead-lag blocks may be utilized to achieve the anti-phase. Additionally, the phase compensation system must account for the phase shift introduced by the various time delays.

The positioning of the pole and the zero will determine at what frequency the phase compensation system provides optimal dampening. Depending on the utilized lead-lag blocks there may be more time constants than T1 and T2 as shown in Figure 4.5 on page 29. All of these constants will be initialized in a Matlab script alongside $T_w$ before simulating the simulation in Simulink. The output of the adopted PSS structure for the WPP POD controller will serve as the stabilizing signal which will dampen out the detected PO.

To highlight where the WPP POD controller will affect the control of the WPP an explanation of a WPP controller is given in the following section.

## 4.7 WPP controller

An overall illustration of a WPP main controller is configured is illustrated in Figure 4.6.

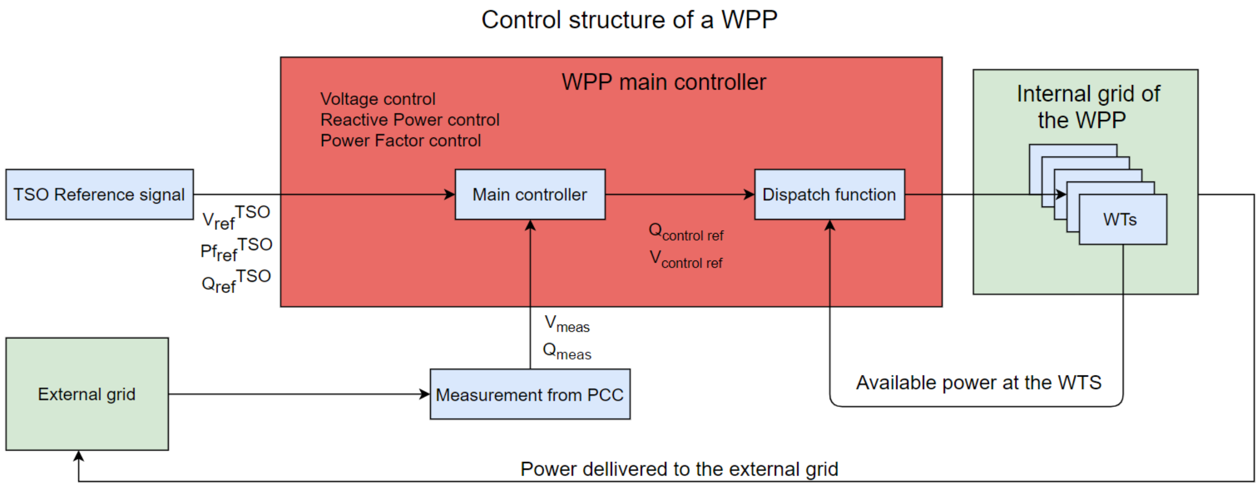


Figure 4.6: Illustration of the overall WPP control structure [30, p. 8].

Observing Figure 4.6 it is shown that the main controller of the WPP can be configured to react on several different inputs depending on the control of the WPP and the reference supplied by the TSO. These references are then delivered to the main controller of the WPP, which treats them and delivers a $Q_{ref}$ or a $V_{ref}$ to the dispatch function of the WPP main controller. However, at the PCC, the POD controller has to identify the PO before it can start acting upon it. This is done by measuring the grid voltage at the PC where the PO is observable. Both an active and reactive power measurement at the PCC will be ill-suited for the identification of the PO as they will appear as constant measurements due to the WPP delivering power to the grid.

Therefore will the WPP POD controller act upon a power calculation which is computed from the voltage and current measurements at the PCC. Meaning if a PO is observed in the voltage and current measurements it translate it into an equivalent power oscillation, which is fed to POD controller, which then in turn will adjust a the reactive power reference given to the WPP. This also implies that the main controller of the WPP will control the reactive power output of the WPP directly. [30, pp. 7-10]

With this in mind the following main reactive power control is illustrated in Figure 4.7.

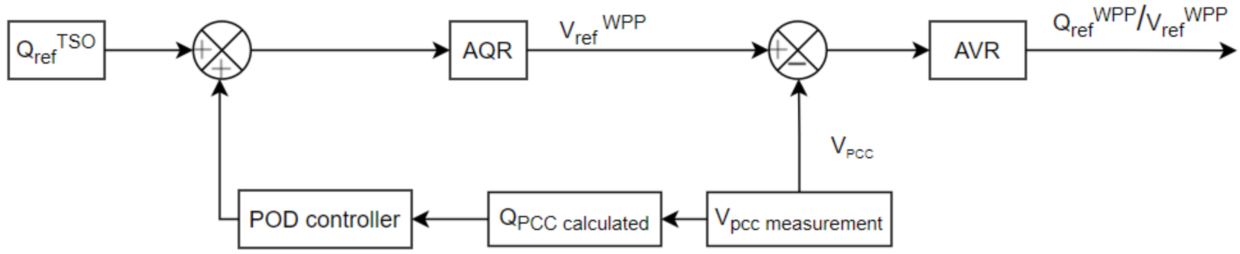


Figure 4.7: Illustration of a configuration for Q-control of the main controller inspired by [30, p. 9].

Investigating Figure 4.7 it is seen that the voltage measurement from the PCC is both delivered to a block that estimates amplitude of the power oscillation before it is given to the POD controller which in turn affects the reactive power reference given to the AQR control. Note the the POD controller output is added to the power reference and not substracted, this is due to the POD controller should produce a signal that is in antiphase with the oscillation. The voltage measurement is also given to the summation block after the AQR control before it is handed over the AVR controller. The AVR controller is implemented after the AWR control to prevent the AQR controller from violating voltage limits with its control indicating the AVR control acts as a protective measure. Whereafter the reference is given to the dispatch function of the WPP main controller. [30, pp. 9-10]

Both the AQR and AVR block takes the form of PI controllers in the s-domain and are part of the main control block in Figure 4.6. The focus of this study is to develop and design a POD controller as an optional control input to the main controller of the WPP, thus no further explanation of the configuration of the AQR and the AVR block is given. For a detailed explanation of AVR and AQR block, and how to tune them the reader is referred to [30, pp. 10-13] & [30, pp. 75-93]. Lastly, the configuration of the dispatch function and how to optimize is also outside the scope of the project. For a detailed description of the dispatch function the reader is referred to [30, p. 13-14]. A summary of all the decisions taken in this chapter is provided in the following section.

## 4.8 Summary of model considerations

In this chapter, the model criteria were described, and from this description, the following model decisions are made.

1. The WT is considered to be a fully rated WT of type 4.
2. The external grid is modeled as a Thevenin equivalent circuit, with consideration to the SCR and XR-ratio.
3. The time delay for the acquisition of measurements at the PCC is 10 ms.
4. The internal time delay of the WTs is 4 ms.
5. The time delay between WTs is 5 ms.
6. The total time delay implemented in the simulation is 91 ms
7. The POD controller will act as an additional option for reactive power control. Thus the controller must start acting upon the PO within 2 seconds and complete its control action with 30 s. Additionally, the rate of change in Q must not exceed 10 MVAr/s.
8. The POD controller is only allowed to act in the 0.2-0.7 Hz range to prevent it from adversely affecting the natural damping of local oscillation performed by SGs.
9. The WPP POD controller will have the structure of a traditional PSS controller, but the phase compensation system will compensate for the lag introduced by time delays.
10. The $T_w$ constant is chosen to be equal to 10.
11. $T_1$ and $T_2$ are designed after the expected PO.
12. The configuration of the main controller block in a WPP is not considered. Meaning a detailed explanation of its configuration options is not explained as it is outside the scope of the study.
13. A detailed description of the AVR and AQR block is not given as these are also outside the scope of the study.

# 5 Simulation description and results

This chapter will describe how the voltage at the PCC is estimated and evaluate the accuracy of this approximation and describe what the introduced power oscillation is modeled after. Additionally, this chapter covers the influence of the implemented time delay and the tuning of the POD controller alongside the evaluation of the performance of the developed POD tune.

## 5.1 Voltage at the PCC

Initially the voltage at the PCC can obtain algebraically by solving the power equations for a two bus system as illustrated in Figure 4.3 on page 25. The two bus system is illustrated again in Figure 5.1 for simplicity where the WPP is considered to be the sending and and the external grid being the receiving end.

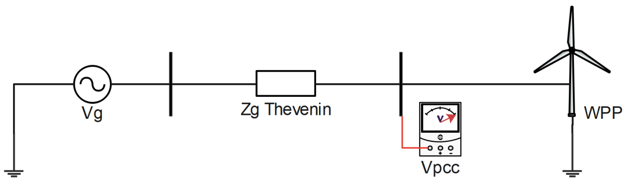


Figure 5.1: two bus system

The SCR ratio and the XR-ratio are used to calculate the grid impedance, resistance, and reactance, which is given in Equation 4.1-4.5 on page 25. The active and reactive power injected by the WPP can be described by Equation 5.1 and 5.2.

$$Q_{WPP} = \frac{V_{PCC}^2 - V_{PCC} \cdot V_g \cdot cos(\delta)}{Z_g} \tag{5.1}$$

$$P_{WPP} = \frac{V_{PCC} \cdot V_g \cdot sin(\delta)}{Z_g} \tag{5.2}$$

$$Z_g = R_g + jX_g \tag{5.3}$$

The active and reactive power injected by the WPP is known alongside the grid voltage ($V_g$), resistance ($R_g$), and reactance ($X_g$) leaving the voltage at the PCC ($V_{PCC}$) and the angle ($\delta$) as unknowns. Equation 5.2 and 5.1 presents a system of equations of two unknowns, which can be solved for $V_{PCC}$ and $\delta$ to ascertain how the voltage at the PCC is affected by the WPP.

Solving Equation 5.2 for $sin(\delta)$ yields the following expression:

$$sin(\delta) = \frac{P_{WPP} Z_g}{V_{PCC} V_g} \tag{5.4}$$

Using the identity $cos(\delta) = \sqrt{1 - sin(\delta)^2}$ it is possible to substitute $cos(\delta)$ in Equation 5.1 with Equation 5.4 resulting in Equation 5.5.

$$Q_{WPP} = \frac{V_{PCC}^2 - V_{PCC} V_g \sqrt{1 - \left(\frac{P_{wpp} Z_g}{V_{PCC} V_g}\right)^2}}{Z_g} \tag{5.5}$$

Observing Equation 5.5 it is seen that the only remaining unknown is $V_{PCC}$, and solving Equation 5.5 for $V_{PCC}$ yields 4 solutions which is given in Equation 5.6-5.7.

$$V_{PCC} = \pm \frac{\sqrt{2V_g^2 + 4Q_{WPP}Zg + 2\sqrt{V_g^4 + 4V_g^2 Q_{WPP} Zg - 4P_{WPP}^2 Z_g^2}}}{2} \tag{5.6}$$

$$V_{PCC} = \pm \frac{\sqrt{2V_g^2 + 4Q_{WPP}Zg - 2\sqrt{V_g^4 + 4V_g^2 Q_{WPP} Zg - 4P_{WPP}^2 Z_g^2}}}{2} \tag{5.7}$$

Inspecting Equation 5.6 and Equation 5.7 two of the solutions can be neglected as the negative solution of Equation 5.6 and 5.7 will predict the voltage at the PCC to be negative, which will never be the case and they are ruled out. That leaves the positive solutions of Equation 5.6, and 5.7 to be investigated. However, before the positive solutions of 5.6 and 5.7 are investigated the behavior of the grid impedance ($Z_g$) is examined when the XR-ratio and SCR-ratio changes.

The magnitude of $Z_g$ is computed as $\sqrt{Rg^2 + Xg^2}$ and it is plotted in Figure 5.2 where XR-ratio is varied from 3 to 10 and the SCR ratio from 3 to 20. Note that the impedance base changes with the rising SCR-ratio as $Z_{base} = \frac{V_{LL\ base}^2}{S_{base}}$ and $SCR = \frac{S}{P_{rated}}$, where the $P_{rated} = 209$ MW and $V_{LL\ base} = 400$ kV, meaning $S_{base} = P_{rated} \cdot SCR$. This means for every XR-value the SCR-ratio is swept from 3-20, thus it is expected that the grid impedance will decline with the rising SCR-ratio.

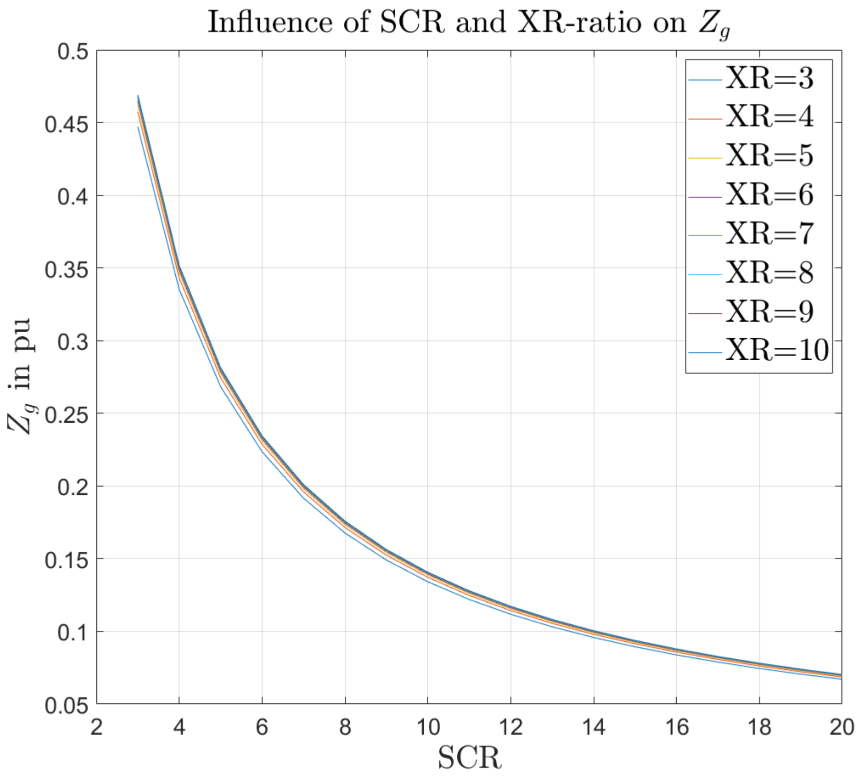


Figure 5.2: Illustration of the magnitude of $Z_g$

Inspecting Figure 5.2 it is evident that it agrees with the expectation, that as the SCR rises the grid impedance decreases. Where the XR-ratio describes the ratio of reactance to resistance.

Reinspecting Equation 5.6, and 5.7 this means that for a stiff grid SCR=20 and XR=10 that the WPPs influence on the voltage the PCC is less compared to a weak grid. Indicating that a weak grid is more susceptible to active and reactive power changes. However, it is still expected that the WPP is bound to force the voltage at the PCC to rise when the WPP injects active and reactive power and it to drop if it consumes power. As the goal for this project is to develop a Q control to perform POD this claim is investigated by fixating the $P_{WPP}$ at 0.5 pu while varying $Q_{WPP}$ from -0.3 to 0.3 pu with a power base of $209MW \cdot 20$ = 4180 MVA and $V_{LL\ base}$ = 400 kV. This produces the following two graphs illustrated in Figure 5.3.

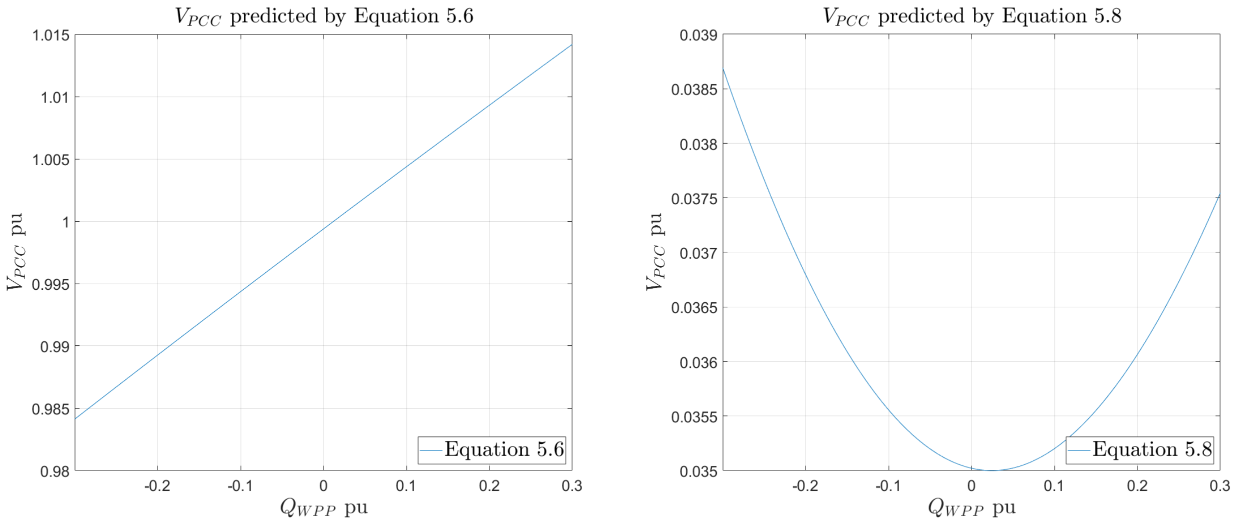


(a) Equation 5.6 (b) Equation 5.7

Figure 5.3: Voltage at the PCC as predicted by Equation 5.6-5.7

Observing Figure 5.3 it is evident that Equation 5.7 depicted in Figure 5.3b should be neglected as well since it predicts $V_{PCC}$ to be far below 1 pu. Where Equation 5.6 depicted in Figure 5.3a shows that $V_{PCC}$ rises when as the WPP goes from consuming to injecting reactive power.

To evaluate the accuracy of Equation 5.6 its behavior is checked against a Gauss-Siedal load flow where the SCR and XR-ratio are varied from 3-20 and 3-10 respectively. Where the WPP is injecting $P_{WPP}$ and $Q_{WPP}$ equal to 0.7 and 0.3 pu respectively of the rated power of the WPP yielding Figure 5.4.

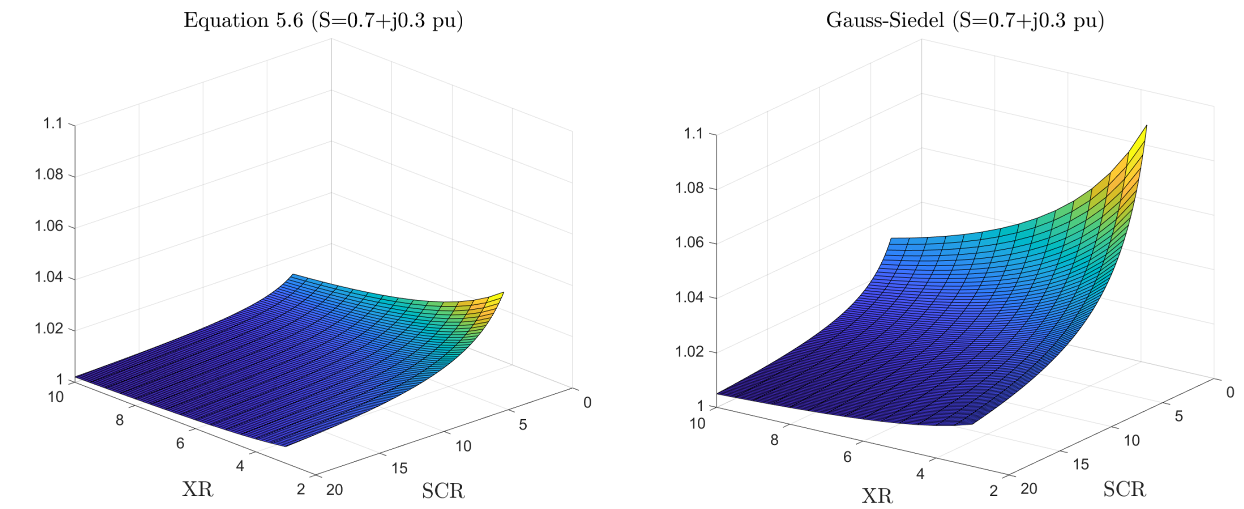


(a) Equation 5.6 (b) Guas-Siedel load flow solution

Figure 5.4: Voltage at the PCC as predicted by Equation 5.6 compared to a Gauss-Siedel load flow

Inspecting Figure 5.4 it is evident that there is a great difference in the predicted value between Figure

5.4a and 5.4b, when the SCR and XR-ratio are low. However for a high values of the SCR and the XR-ratio it is observed that both Equation 5.6 and the load flow solution depicted in Figure 5.4 both approach 1 pu. Indicating that Equation 5.6 for grids which SCR and XR-ratio above 16 and 6.5 respectively can be used to predict the voltage at the PCC. This claim is backed up by computing the % difference between Equation 5.6 and the Gaus-Siedel load flow illustrated in Figure 5.5.

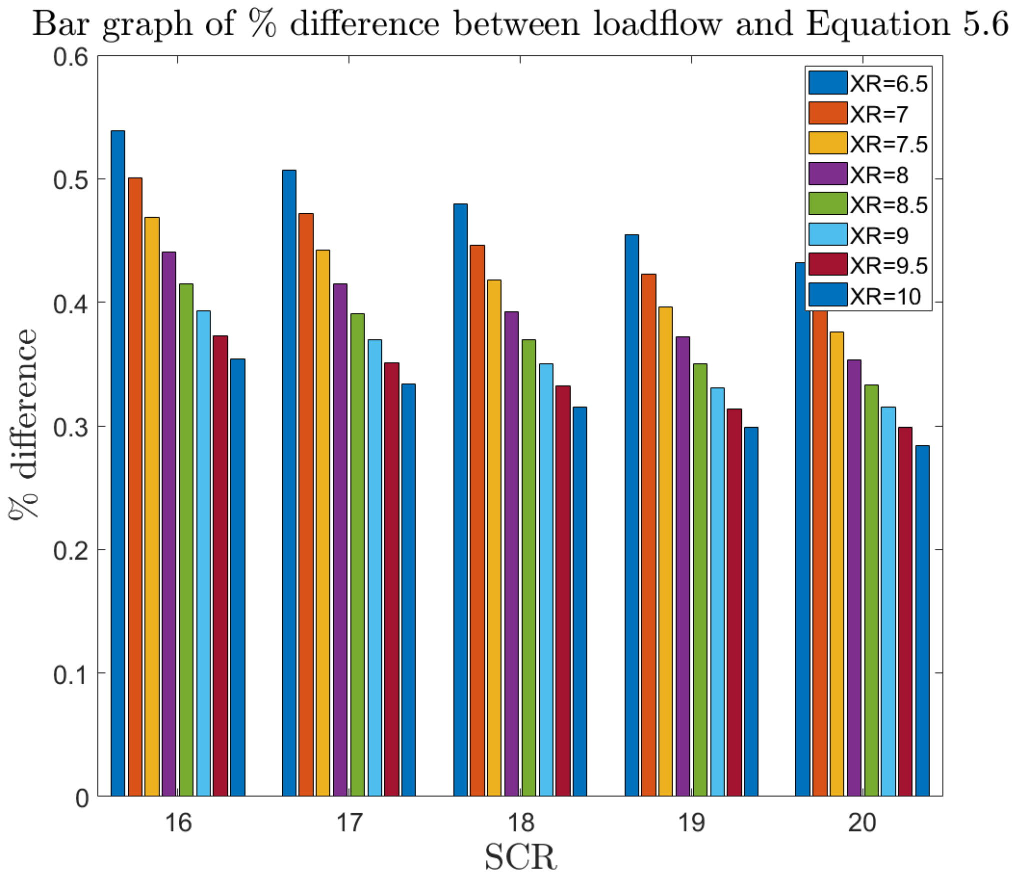


Figure 5.5: Illustration of the % difference between the load flow solution and Equation 5.6

From Figure 5.5 it is clear that the difference between equation 5.6 and the load flow solution shown in Figure 5.3 for grids above a SCR of 16 and XR-ratio above 6.5 is 0.55% or below. Therefore is Equation 5.6 accurate enough to be used to predict the voltage at the PCC for the POD controller when tuning it. A table of the % difference for a wider range of SCR and XR-ratio is provided in Appendix A

In the coming section, the signal which the POD controller is tuned after is described and what event the PO is based upon.

## 5.2 The ideal PO signal

Article [7] in Section 1.4 on page 6 was used to identify the different observed POs present in the CE power grid. These two articles identify 4 global modes where global mode 4 is of interest for this study as it involves a north-south oscillation. However, a more recent event with PO on the north-south axis will be utilized as a baseline which occurred in 2017.

The PO event observed on the 3'rd of December 2017 involved an oscillation between the southern power plants of Italy, SE European countries, Southern France and Switzerland were swinging against Northern Europe ( Germany, Denmark, and France), falling within the Global mode 4 north-south oscillation as described article [7]. This oscillation had an amplitude of ±200 MW per line resulting in the PO exceeding 1 GW at a frequency of 0.29 Hz. This PO caused to voltage in the middle of the CE grid to oscillate with ±2.5 kV and even worse voltage oscillation on the Italian peninsula ranging from +7 to -12 kV. [35, pp. 8-10] The PO illustrated in Figure 1.4 on page 6 and the PO observed in the report [35, pp.9-10] exhibits a behavior, which resembles a standard second-order transfer function with low damping and a low natural frequency. Thus, a simple way of approximating POs can be done by utilizing Equation 5.8.

$$PO = \frac{\omega_n^2}{s^2 + 2\zeta\omega_n s + \omega_n^2} \tag{5.8}$$

Where $\zeta$ describes the damping of the oscillation and $\omega_n$ describes the frequency of the PO.

The event in [35, pp.9-10] will serve as a baseline for constructed PO utilized to tune the POD controller after. A voltage deviation of $\Delta$ 19 kV corresponds to 0.0475 pu on a base of 400 kV, and the PO will have a frequency of 0.29 Hz. Additionally, it is assumed that it is an ideal true RMS measurement, meaning the voltage before the PO will be very close to 1 pu, and therefore is the PO centered around 1 pu. this produces the voltage PO observed in Figure 5.6, which is used to tune the POD controller after.

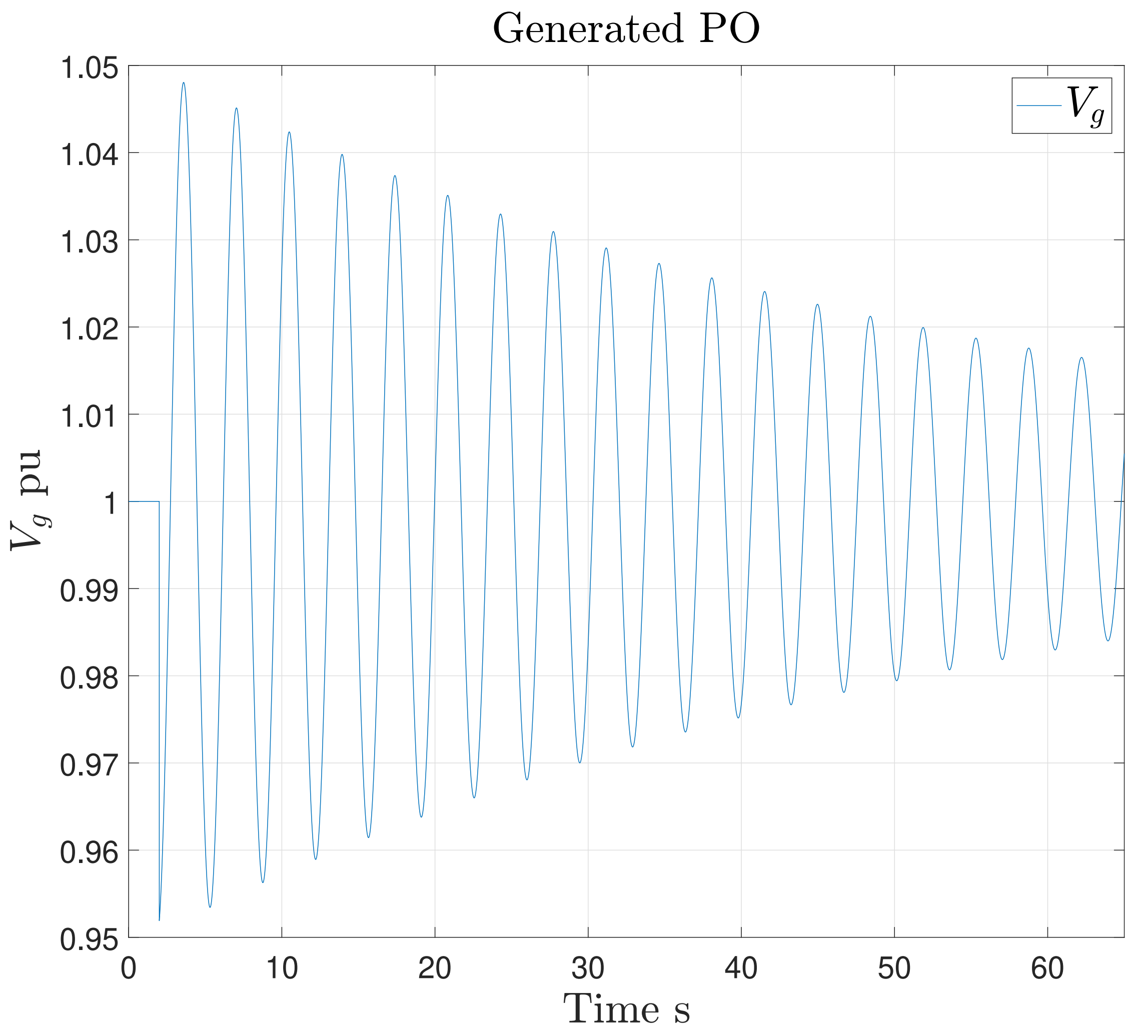


Figure 5.6: The generated voltage oscillation.

By adjusting $\omega_n$ and $\zeta$ in Equation 5.8 on the preceding page it is possible to adjust the damping, frequency, and time frame of the generated oscillation, thereby making it easy to check the performance of the POD controller over multiple frequencies. As the POD controller is to act on the reactive power reference of the WPP the generated PO in voltage needs to be translated into its equivalent amplitude in power which is done by executing Equation 5.9 through 5.11 in matlab

$$|Ig| = \frac{|V_g|}{|Zg|} \tag{5.9}$$

$$|S_g| = abs(I_g V_g) \tag{5.10}$$

$$\tag{5.11}$$

Thus the oscillation in apparent power is illustrated in Figure 5.7

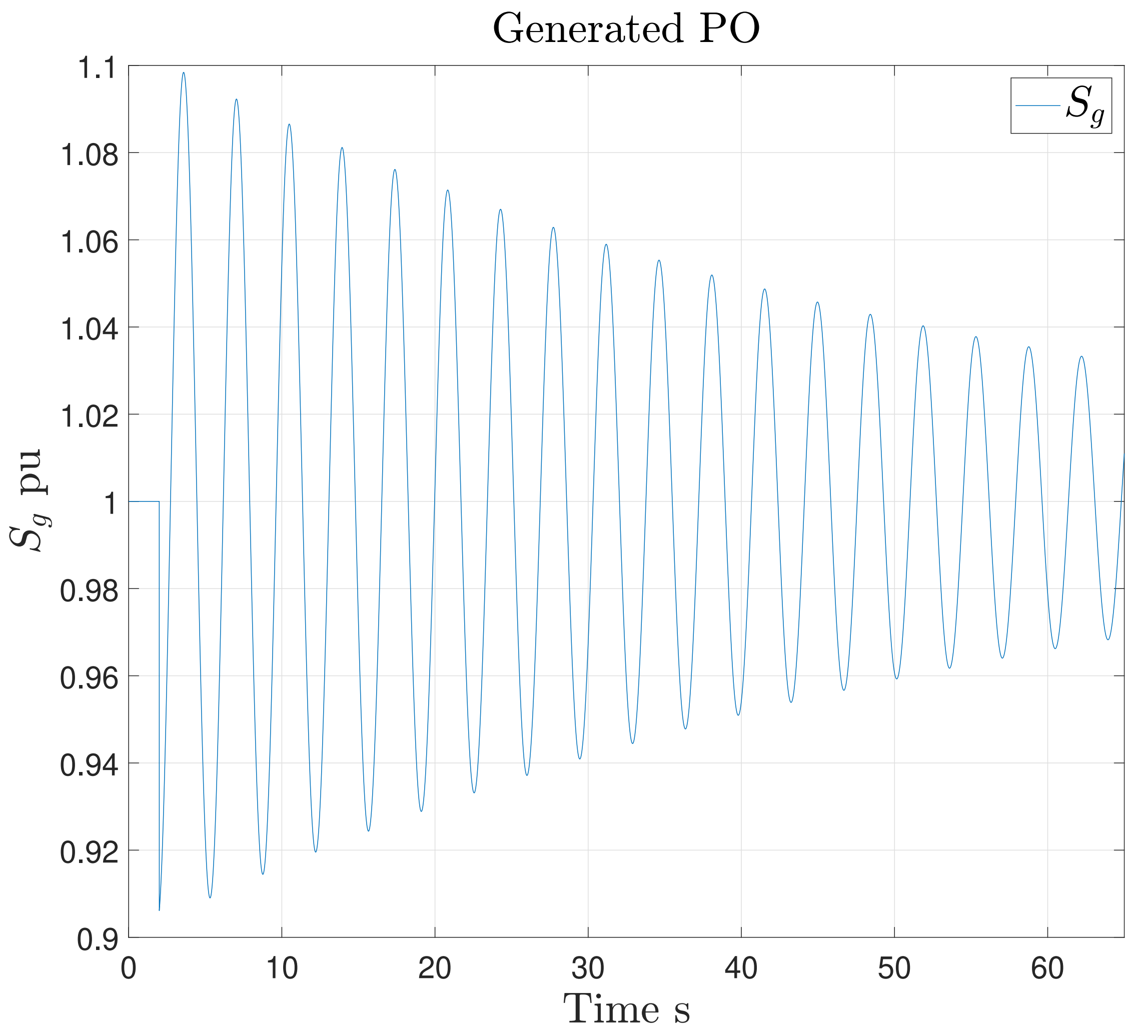


Figure 5.7: The absolute apparent power oscillation.

## 5.3 Effect of the time delay

The first part of the tuning is to identify how much phase lag the measurement and communication delay introduces to the system. The generated signal with a time delay of 91 ms is shown in figure Figure 5.8. The generated PO signal has a frequency of 0.29 Hz, which means it has a time period of $T = 1/f_n = 3.448s$. In order to find how many degrees of lag a time delay of 91 ms introduces it is first calculated how many milliseconds 1° corresponds to by using Equation 5.12.

$$\frac{ms}{\circ} = \frac{3.448 \cdot 1000}{180^\circ} = 19.15\ ms/^\circ \tag{5.12}$$

Knowing how many milliseconds corresponds to 1° it is possible to calculate the phase lag a delay of 91 ms introduces to the system by using Equation 5.13

$$
\begin{aligned}
Phase\ shift &= \frac{Time\ delay}{Time\ per\ degree} \\
&= \frac{91ms}{19.15\frac{ms}{\circ}} = 4.75°
\end{aligned}
\tag{5.13}
$$

So the controller needs to account for a total phase shift of 184.75° to achieve anti-phase and compensate for the 4.75° phase shift introduced by the time delay introduced by the measurement and communication delay.

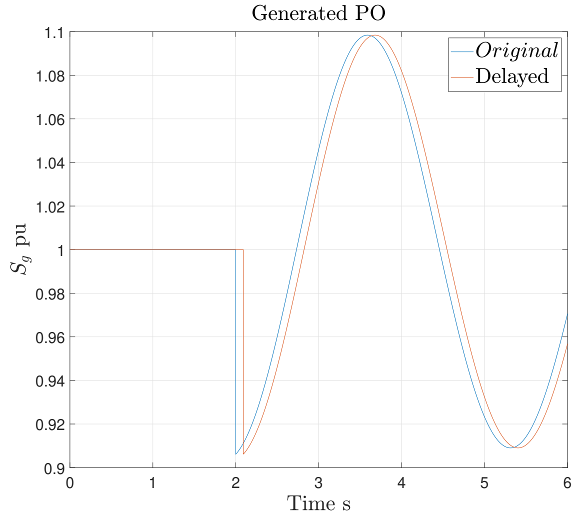


Figure 5.8: Illustration of the 91 ms time delayed signal

## 5.4 Tuning of the POD controller

This section will highlight the tuning procedure of the POD controller and its sensitivity.

The POD controller is tuned by placing the poles and zeros to obtain the desired phase shift at the frequency of the generated PO signal, which is 0.29 Hz. If the anti-phase is to be achieved with lead-lag blocks 3 of them are needed to be deployed to achieve the anti-phase of 180° where the last lead-lag block will account for the 4.75° phase shift the time delay introduces.

However, the anti-phase can also be achieved by utilizing negative feedback instead of lead lags blocks. Using this approach only one lead-lag block needs to be tuned to achieve the desired behavior at a certain frequency. The pole of the lead-lag block is placed one decade before it is supposed to be active placing the pole at 0.0029 initially. The placement of the zero is calculated based on the desired phase shift, which is affected by the total time delay in the system. The zero is then calculated by solving Equation 5.14 for $\omega_1$. The Laplace operator is equal to $s = j\omega$.

$$Desired\ phase\ compensation = \frac{1 + \omega_1 \cdot s}{1 + 0.029s} \tag{5.14}$$

$$solve\ 0.0829 = atan\left(\frac{imag(\frac{1+j\omega_1}{1+j*0.029})}{real(\frac{1+j\omega_1}{1+j*0.029})}\right), \omega_1 \tag{5.15}$$

From 5.15 $\omega_1$ is found to be equal to 0.1124, and the final form of the lead lag block that acquires 4.75° phase is depicted below:

$$Lead\ lag\ block = \frac{1 + 0.1124s}{1 + 0.029s}$$

The gain for the POD controller is then identified by investigating the controller with a root locus and bode diagrams illustrated in Figure 5.9 and 5.10

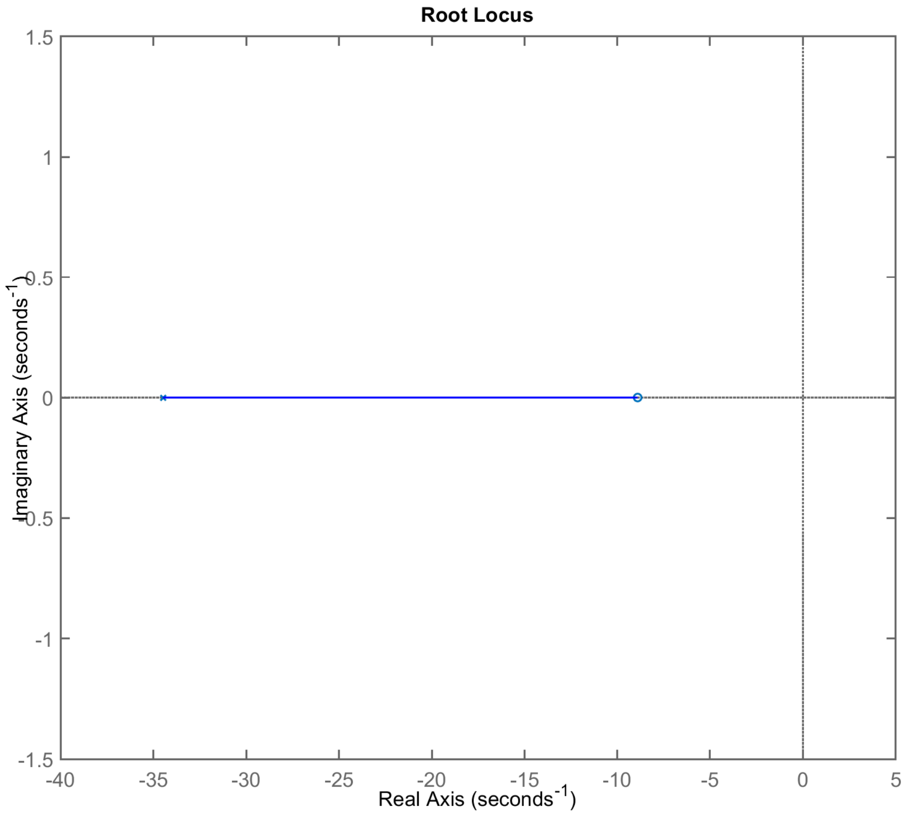


Figure 5.9: Illustration of the closed loop stability of the tuned controller

From the root locus diagram in Figure 5.9 it is clear that both the pole and the zero are located in the left half-plane indicating a stable controller. The zero is located at -8.9 rad and the pole is located at -34.5 rad.

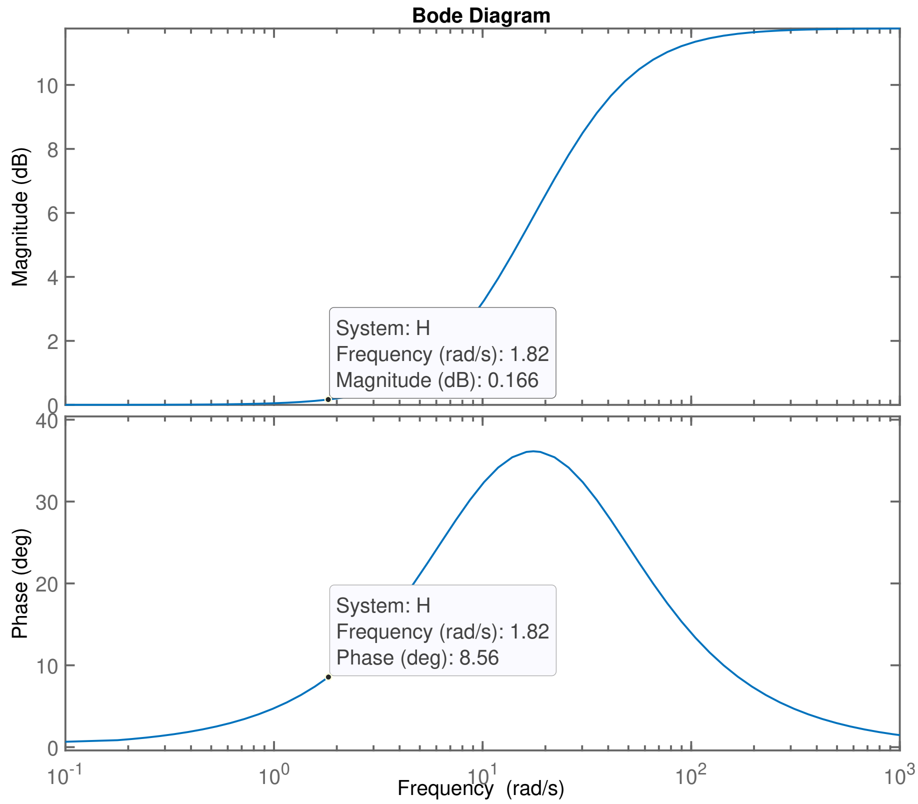


Figure 5.10: Illustration of the bode plot for the tuned controller

From the bode plot in Figure 5.10 it is spotted that at the desired frequency of 1.82 rad/s (0.29 Hz) that the phase compensation is 8.56°, which is double of the desired compensation. Therefore is the location of the zero readjusted to be located at -13.33 rad instead to achieve the desired 4.75° phase shift, and a new bode plot is constructed where the gain is read out in the same manner as illustrated in Figure 5.10. The gain to be implemented into the Simulink model is then found by using equation 5.16.

$$gain = 10^{\frac{0.0683}{20}} = 1.00789 \tag{5.16}$$

Having acquired an initial tune for the POD controller is implemented into a simulation environment in Simulink to investigate the performance of the initial tune.

### 5.4.1 The Simulink model

In order to test the POD design, it is implemented in Simulink illustrated in Figure 5.11

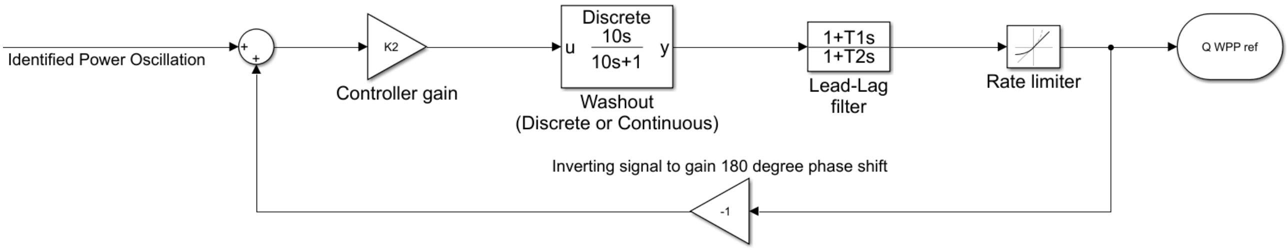


Figure 5.11: Illustration of the POD control structure implemented in simulink

However, a few considerations have to be explained. The simulation is evaluated on the grid's power base of 4180 MVA. Thus, if the WPP is only allowed to change its reactive power output with 10 MVA/s it results in it can only inject 0.0024 pu/s as seen from the grid. Additionally, the simulation is initialized such that the WPP is injecting 0.025 pu active power on the grid's power base. Meaning the reactive power reserve available to dampen any PO is 0.015 pu.

To ensure these considerations are being kept the POD controller is equipped with a rate limiter to ensure the WPP cannot ramp its output with more than 0.0024 pu/s, and a saturation block is included to prevent the controller to ask for more than 0.015 pu reactive power to prevent the controller from asking for more than the available reactive power reserve.

With these considerations implemented the following result illustrated in Figure 5.12 is obtained.

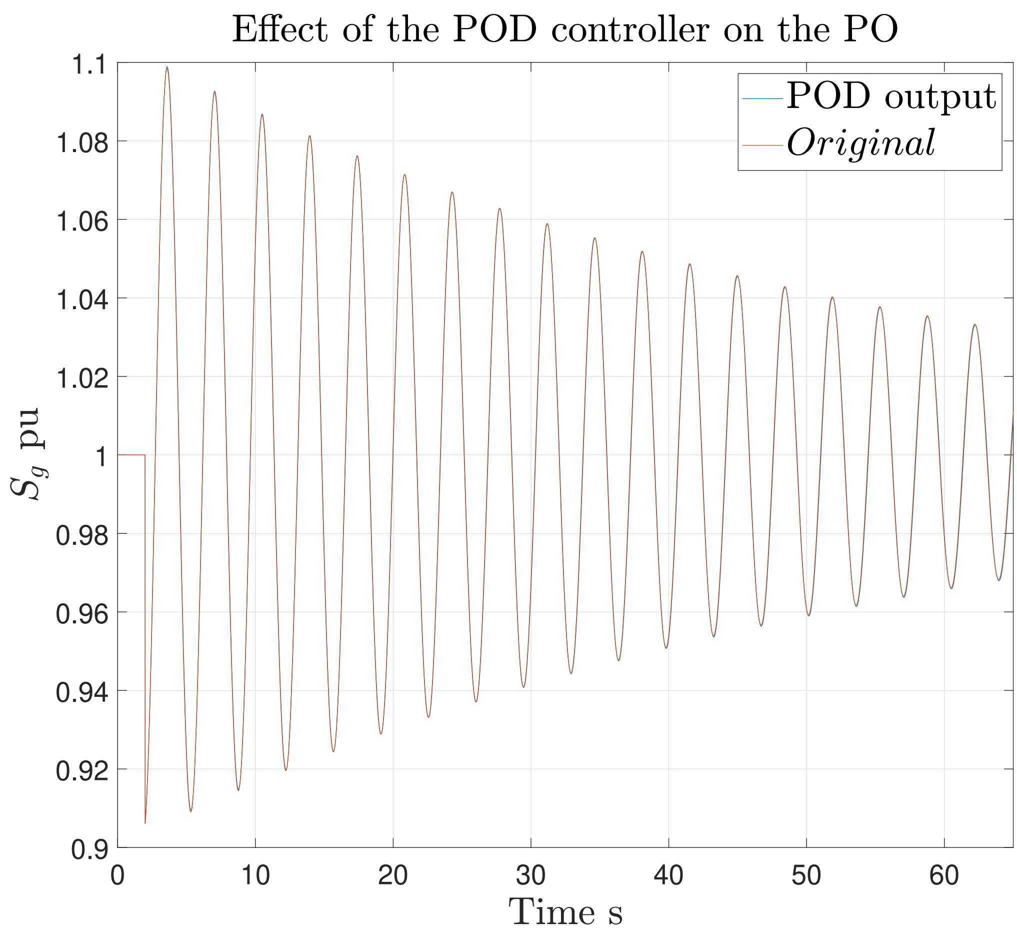


Figure 5.12: Illustration of the Q output with rate limiter

From Figure 5.12 it is evident if the POD controller is to agree with the rate limit of 10 MVA/s from the grid codes corresponding to a change of 0.00239 pu on the grids power base of $S_{base}$=4180 MVA. However, if the rate limit from the grid codes is ignored it is possible to achieve damping as illustrated in Figure 5.13.

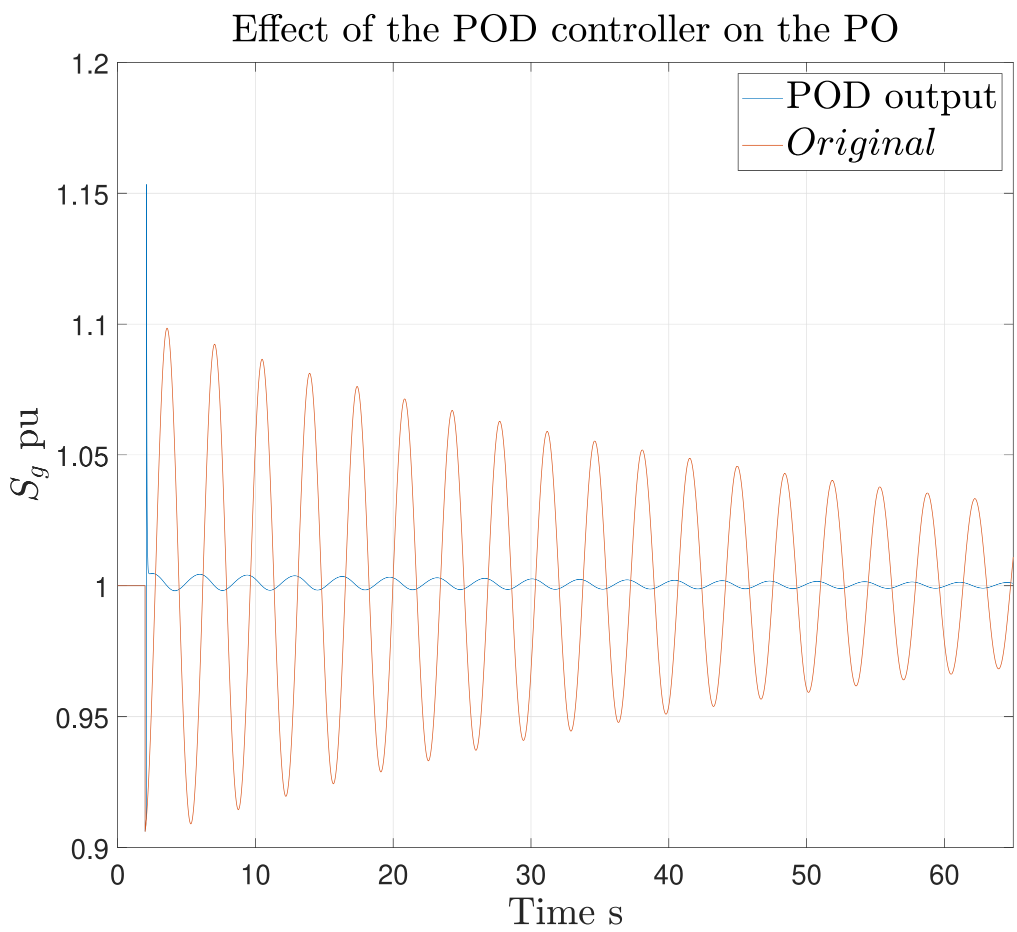


Figure 5.13: Illustration of the Q output without the rate limiter block

In Figure 5.13 the open-loop performance of the POD controller is shown, and damping is achieved. Having shown that the controller behaves as intended, its performance is evaluated in a closed-loop setup to see if it continuously reduces the PO. To prevent the POD from being able to adjust its output instantaneously the rate limiter is reintroduced into the loop, but the rate limit is changed to provide adequate damping. This means that the POD controller should dampen the PO with 5% resulting in a 32% damping of the initial peak after three oscillation periods. This implies that the initial voltage peak of 1.088 pu should be reduced with 0.028 pu after three oscillation periods. The rising and falling slew rate implemented in the rate limiter block is found through trial and error and is set to 0.04 pu to achieve adequate damping of the introduced oscillation. This value, however, is also 17 times greater than the allowed rate limit of 10 MVA/s (0.0023 pu/s) set by the grid codes. The performance of the POD controller is illustrated in Figure 5.14 alongside the prediction of the voltage at the PCC by utilizing Equation 5.6 compared to the original voltage oscillation.

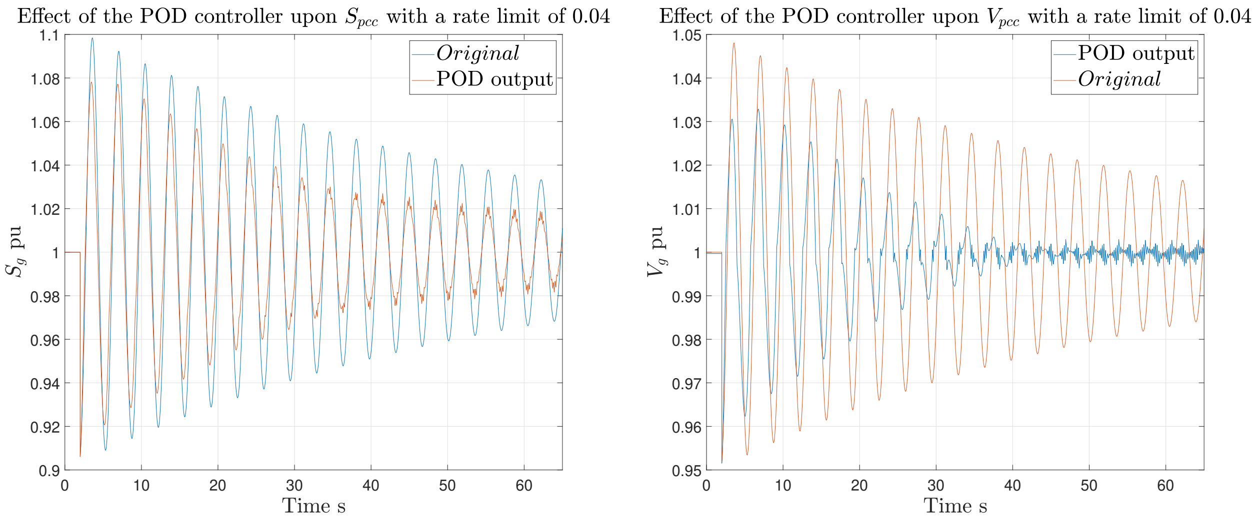


(a) S at PCC

(b) $V_{pcc}$ predicted by Equation 5.6

Figure 5.14: Effect of the POD controller upon the introduced PO

From Figure 5.14 it is observed that the voltage PO at the PCC is damped as a result of the POD controller acting upon the reactive power oscillation. Additionally, it is observed that the output of the POD controller is in phase with the original oscillation shown in 5.14a, but that it is damped adequately as expected. It is also noticed in Figure 5.14b that the damped voltage PO is not completely in phase with the original PO. It is argued the cause of this phase mismatch is caused by the rate limiter as it forces the output of the POD controller to assume a triangular waveform. Additionally, it is seen that the voltage signal predicted by Equation 5.6 becomes distorted as the oscillation is damped below 1.01 pu, however, it is argued that this voltage distortion is within acceptable limits as it is below 1.01 pu.

It also has to be mentioned that the power oscillation is not introduced on top of a 50 Hz signal. For the result shown in Figure 5.14 it has been assumed that the measurement at the PCC is an ideal RMS measurement, meaning no distortion present from the fundamental grid frequency.

Additionally, the performance of the POD controller is only checked for a single frequency, and not evaluated for the entire span of inter-area frequencies, and if it performs adequately if fed a PO with a different frequency.

# 6 Validation model

This chapter will describe the model used to validate the POD controller. The model has been developed through the Ph.D. doctoral course [36] at Aalborg university, and not developed in this project.

## 6.1 Validation model description

A drawn illustration of the model is given in Figure 6.1 where it is observed that the original model contained two WTGs separated by a transmission cable modeled as a pi section. Additionally, the voltage source used to generate the voltage control reference for the controllable voltage sources is based upon standard EN61000-2-2. The voltage source is given the peak voltage amplitude, the base frequency, and phase and output the voltage control reference, which is fed to the controllable voltage sources in the model. All reference signals are marked as red lines, and all physical signals are marked as black lines.

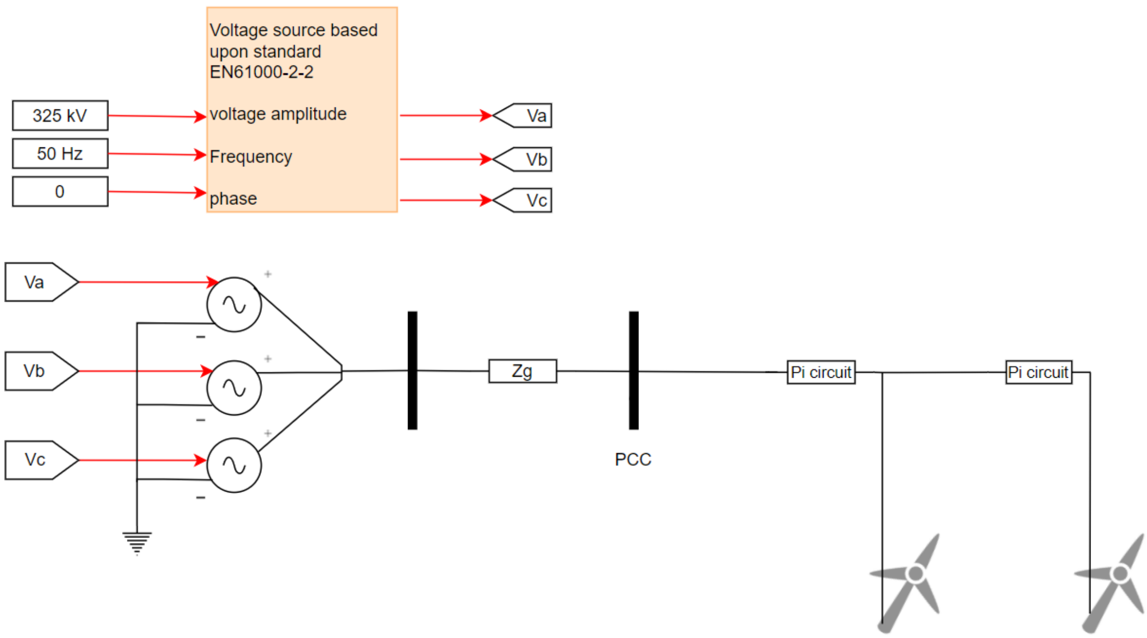


Figure 6.1: Illustration of the validation model

However, as the goal is to validate the performance of the POD controller the model is simplified to only contain one aggregated model of the WPP connected directly at the PCC in Figure 6.1. This means the internal transmission path of the WPP is neglected as it is assumed that the angle of separation between the individual turbines is small enough to allow for a uniform response at the PCC. This simplification is based upon the research done in Article [20], where it was found that for both active and reactive power modulation used to dampen PO's did not cause the angle of separation to become too great to prevent a uniform response at the PCC. The reduced model is illustrated in Figure 6.2.

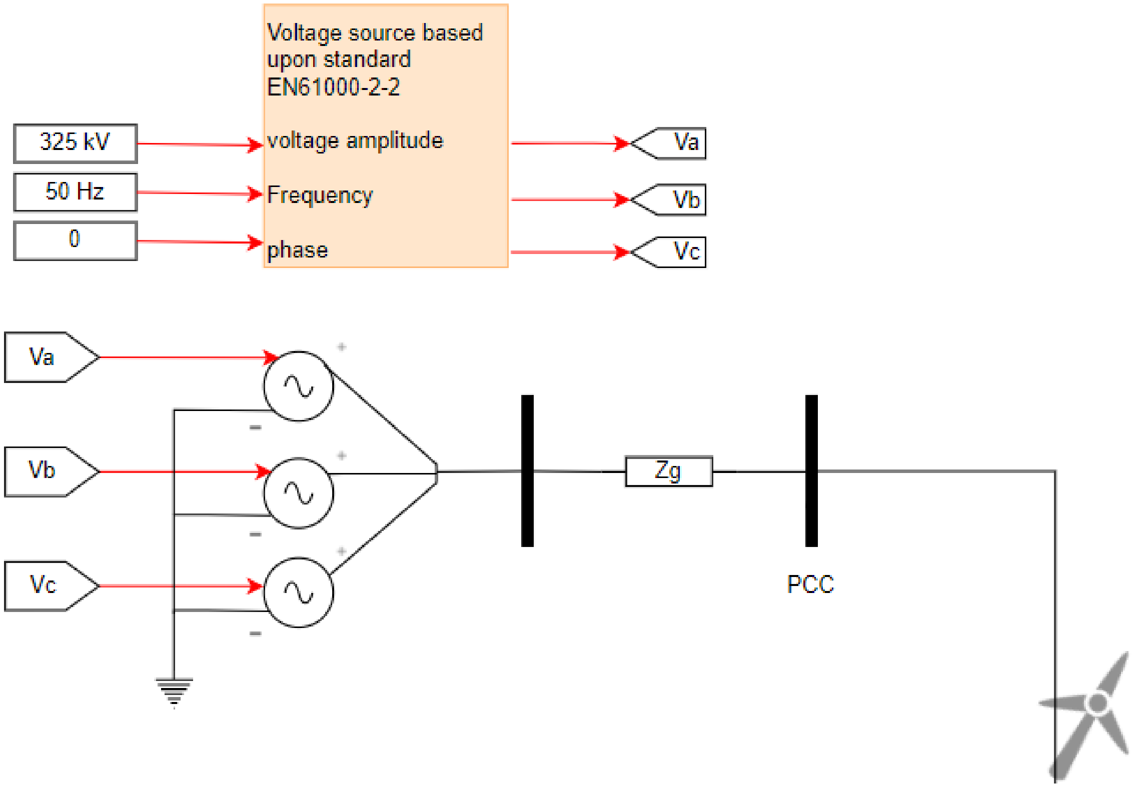


Figure 6.2: Illustration of the validation model

The grid impedance $Z_g$ illustrated in Figure 6.2 covers both the grid reactance and resistance, however, in the Simulink environment it has to be implemented as an RLC branch. This gives rise to some issues as $Z_g$ is the thevenin equivalent impedance of the grid, meaning it is not possible to distinguish the size of inductive to the capacitive element of the reactance. Additionally, the distance element of $Z_g$ is also difficult to ascertain, thus an assumption is made.

It is assumed that $Z_g$ can be approximated as a short transmission line, meaning the capacitive element of the reactance can be neglected and the reactive element of $Z_g$ can be modeled as purely inductive reactance. However, this is a simplification as it is difficult to decide the distance of the equivalent impedance, which may affect the performance of the controller.

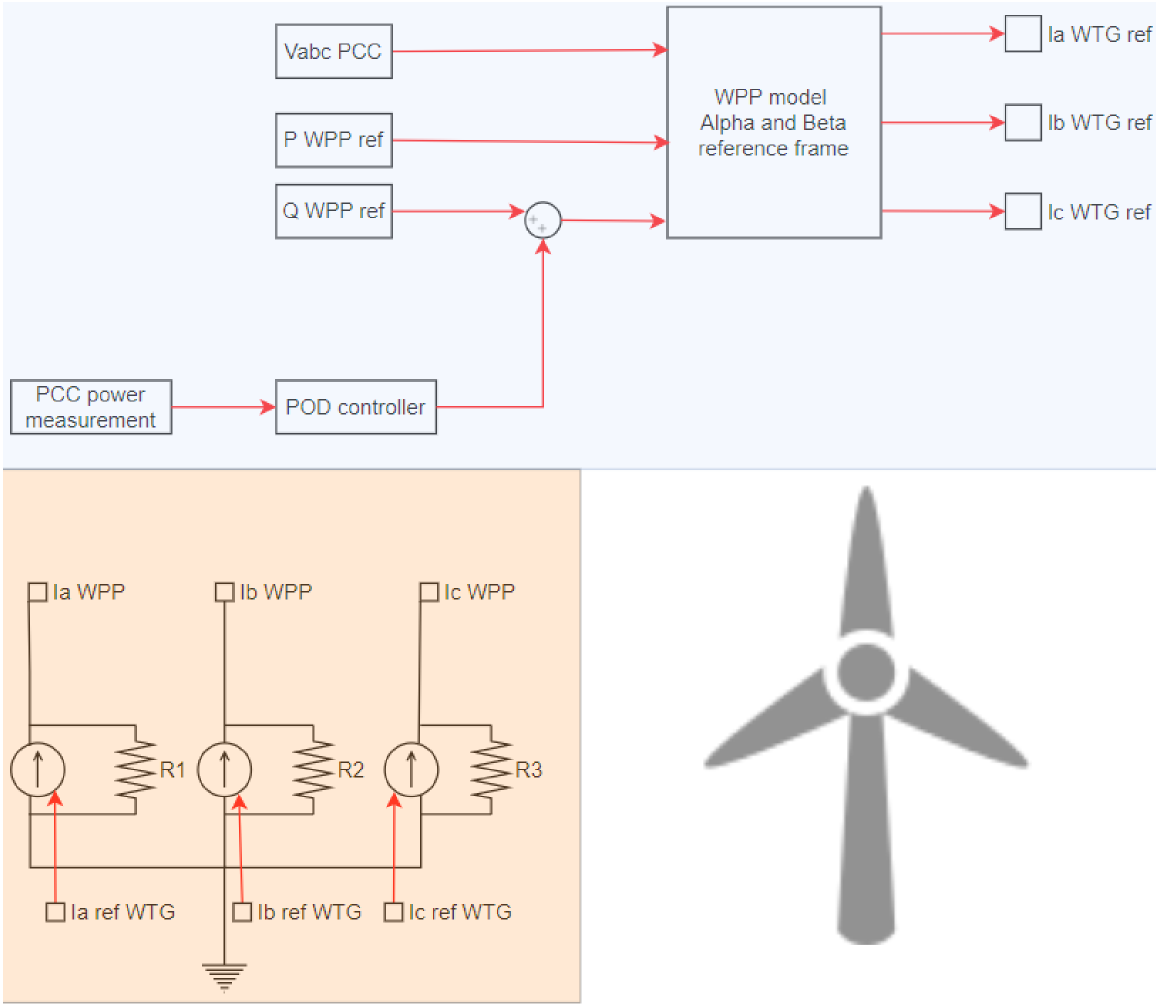


Figure 6.3: Illustration of the validation model

The internal physical and control loop of the WPP is illustrated in Figure 6.3. Where it is observed that the WPP internal control loop operates in the $\alpha\beta$ reference frame which is fed a voltage measurement alongside the P and Q reference for the WPP to produce the $I_{abc}$ reference marked by the blue area of Figure 6.3. Given to the current sources representing the WPP in the orange area of Figure 6.3. The POD controller is implemented to act upon reactive power reference of the WPP after it identifies the PO in the power measurement from the PCC.

With the validation model explained the POD controller is implemented and its performance is tested against a PO with a frequency of 0.29 Hz, and the results are presented in the coming section.

## 6.2 Evaluation of the POD controller performance

The model is initialized with the following parameters in the simulation environment.

| Name | Value |
|---|---|
| $Z_g$ | 3.8088 + j38.0875 Ω |
| $R_g$ | 3.8088 Ω |
| $L_g$ | 0.1212 H |
| $V_g$ | 325 kV |
| $P_{WPP}$ ref | 104.5 MW |
| $Q_{WPP}$ ref | 62.7 MVA |
| Rate limit | 0.04 pu/s (167.2 MVA/s) |
| Saturation limit | ± 104.5 MVA |
| K1 | 3 |
| K2 | 1.00789 |
| K3 | -1 |
| K4 | 4180 MVA |
| Tw | 10 |
| T1 | 0.075 |
| T2 | 0.029 |
| Step time | 5 s |
| Step amplitude | 0.0475 |
| Simulation time | 65 s |

Table 6.1: initialization parameters

It is noticed in Table 6.1 that saturation limit is implemented. This is done to prevent the controller to ask for more power than the WPP plant can provide. Additionally, it has the benefit of providing the controller with anti-windup. For simplicity, a more detailed drawing of the controller and the addition of the saturation block is given in Figure 6.4.

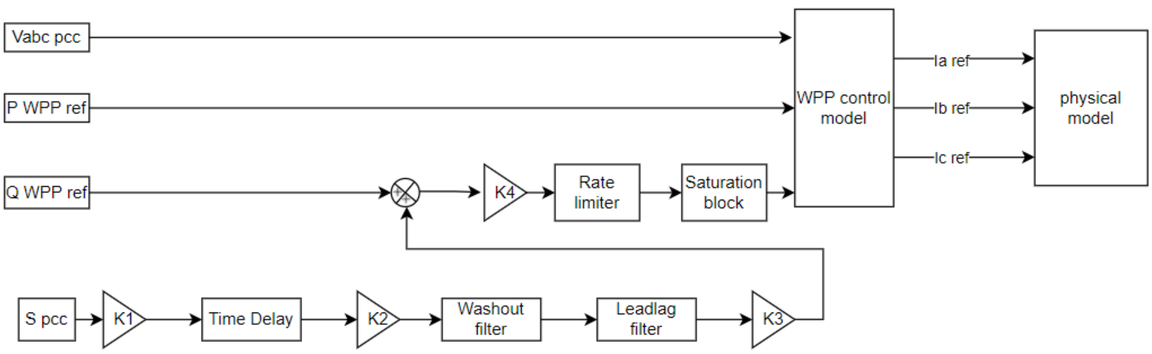


Figure 6.4: Illustration of the implementation of the rate limiter and saturation block.

From Table 6.1 and Figure 6.4 it is observed that the power measurement $S_{PCC}$ is multiplied with K1 it is done so as the system is a balanced three-phase system and S is estimated from a single RMS phase measurement of current and voltage at the PCC.

The PO is implemented in the validation model as an oscillation in the voltage reference for the voltage source as illustrated in Figure 6.5.

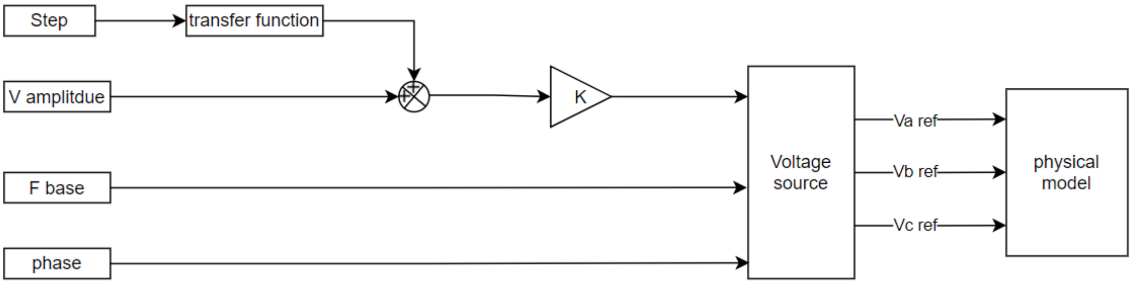


Figure 6.5: Illustration of where the PO is introduced in the validation model

Where the Step block in Figure 6.5 has an amplitude of 0.0475 pu and transfer function as described by Equation 5.8 given in Section 5.2 and the gain K is 325 kV. This produces an identical oscillation to the voltage oscillation illustrated in the Figure 5.6 on page 41 which is then multiplied with the gain of 325 kV and fed to the voltage source.

The voltage before the grid impedance corresponding to $V_g$ is measured and the voltage at the PCC to ensure that the voltage at the PCC is of a higher potential compared to $V_g$. This is checked to ensure the power flow is from the WPP to the grid, and not from the grid to WPP. This result is illustrated in Figure 6.6, where it is observed that $V_{PCC}$ does have a higher potential. Additionally, it is noticed that there is a slight jump in the oscillation at the PCC, however, it is argued that this jump is caused by the way the PO is initialized which acts as an instantaneous jump.

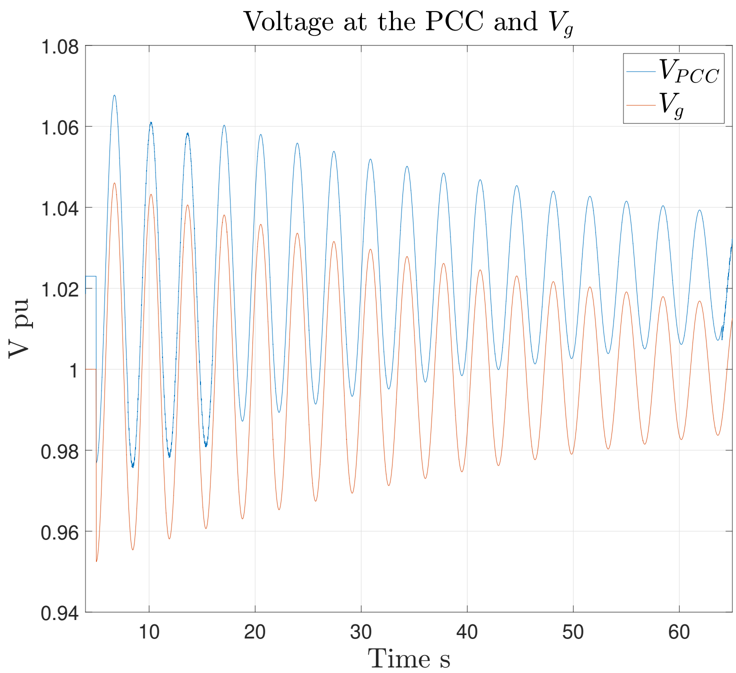


Figure 6.6: Illustration of voltage potential is higher at the PCC.

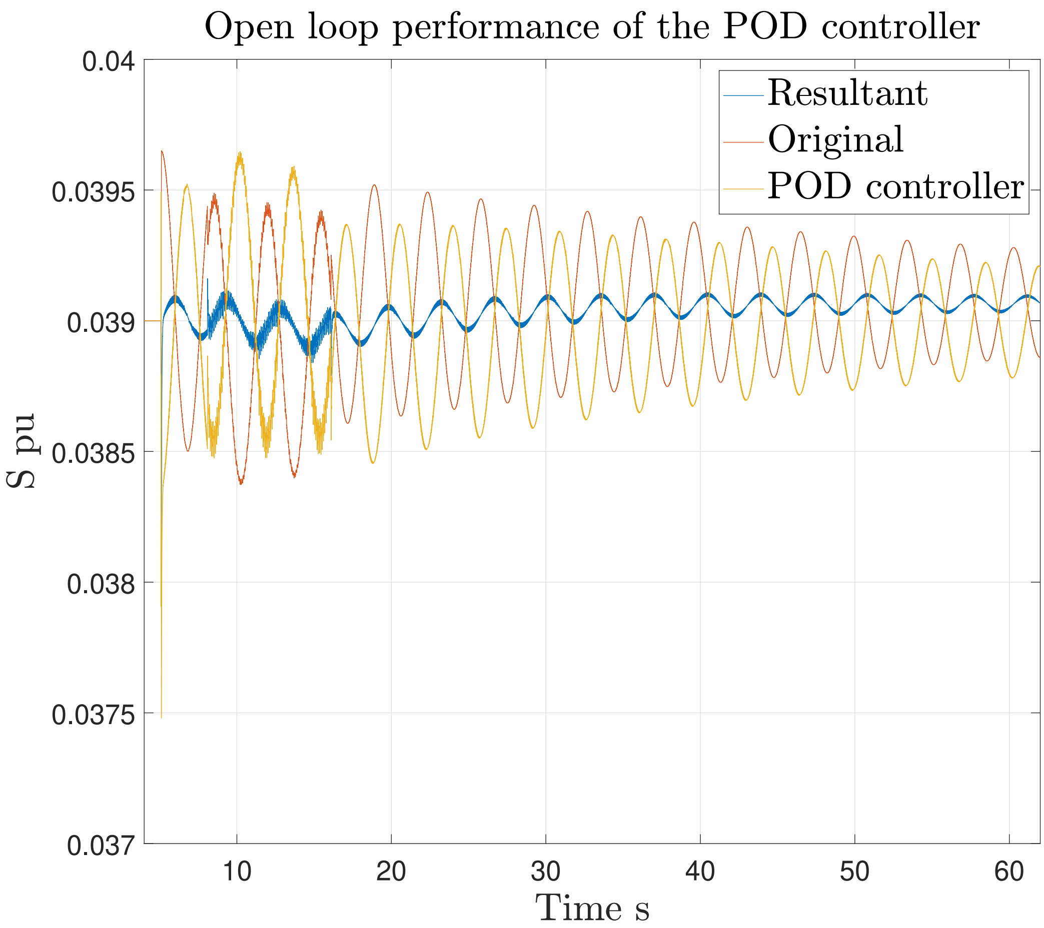


Figure 6.7: Illustration of the open loop performance of POD controller

Next, the open-loop performance of the POD controller is checked in the validation environment to ensure it still achieves anti-phase when fed a signal from the validation model. The result is illustrated in Figure 6.7. In Figure 6.7 it is observed that POD controller output is in anti-phase with the original signal as expected. Additionally, it is noted that the resultant signal damped significantly compared to the original signal when the controller is fed a non-ideal signal.

Next the closed loop performance of the POD controller is evaluated with the proposed rate limit of 167.2 MVA/s as it was given in Table 6.1 the result is shown in Figure 6.8.

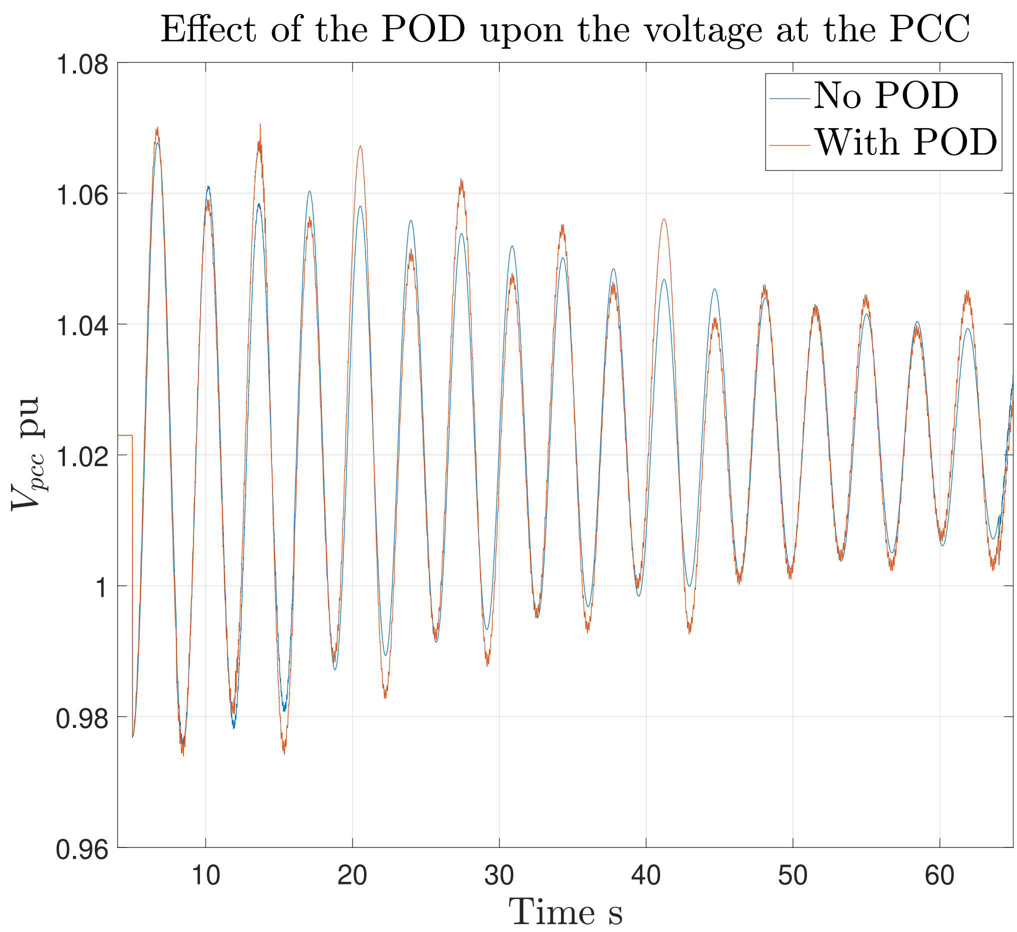


Figure 6.8: Illustration of the closed loop performance POD controller

Where it is observed that some damping is achieved over time, however, it is also observed that the voltage at the PCC experience high voltage spikes when the POD controller acts upon the oscillation. Because of this behavior, it is checked if the rate limit is reduced if it solves the issue and if it achieves better damping before it is evaluated if the POD controller achieves adequate damping. It is decided to test 4 additional rate limit values given in Table 6.2.

| Rate limit value | unit |
|---|---|
| 80 | MVA/s |
| 40 | MVA/s |
| 20 | MVA/s |
| 10 | MVA/s |

Table 6.2: The tested rate limit values

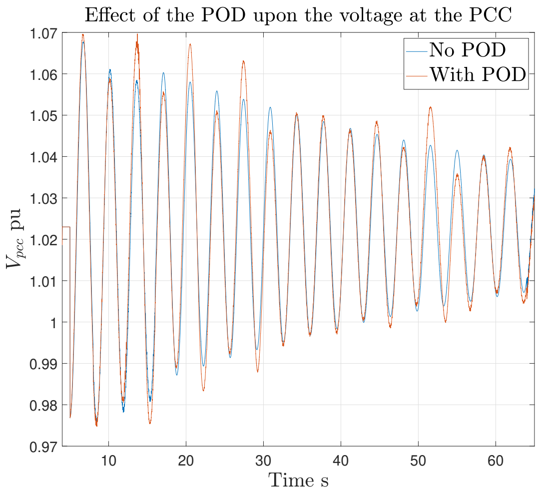


(a) Rate limit 80 MVA/s

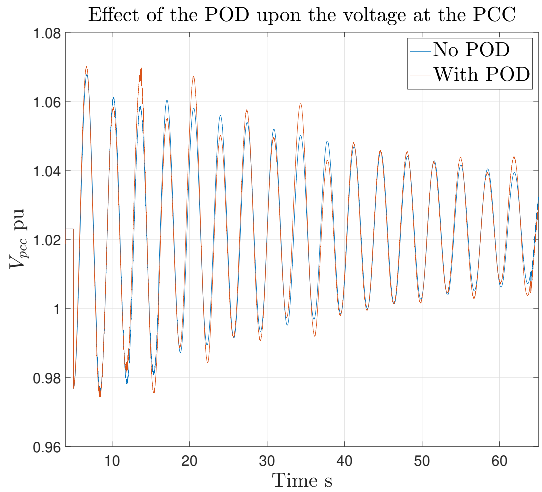


(b) Rate limit 40 MVA/s

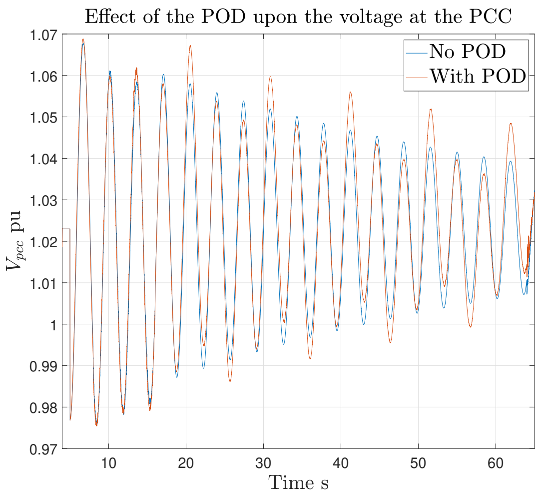


(c) Rate limit 20 MVA/s

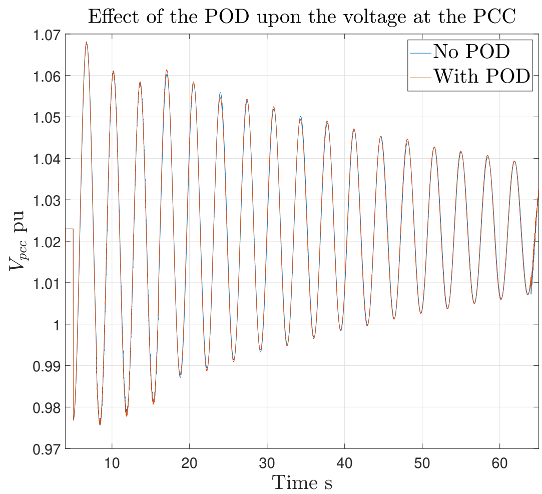


(d) Rate limit 10 MVA/s

Figure 6.9: Illustration of the effect of the different rate limits given in Table 6.2

From the investigation of the different rate limit values illustrated in Figure 6.9 it appears that the rate limit which achieves the most consistent damping is a rate limit of 20 MVA/s. However, it is also evident that voltage spikes are not removed by adjusting the rate limit value it only appears to shift when it occurs. I.e. in Figure 6.9a it is observed that the voltage spike appears to occur every second peak wherein Figure 6.9c it appears to occur every third peak. Additionally, it is observed when investigating Figure 6.9d it is seen that no damping of the PO is achieved, but the voltage spike disappears. It is hypothesized that these voltage spikes may be caused by the controller hitting its saturation limit. This hypothesis is investigated, however, it does not remove the voltage spike, and it is therefore discarded.

Lastly, observing Figure 6.9c it is estimated that the controller does not achieve adequate damping, as it is evident from the graph that it does not dampen the oscillation with 33% within 3 periods as every approximately 3 oscillation period the controller introduces a voltage spike that is higher than PO amplitude. However, overall it appears that the POD controller does achieve some damping in Figure 6.9c, thereby validating the controller. But it also has to be mentioned that the controller does not perform to expectation as it is far less effective than expected.

With the POD controller validated a discussion of the overall results acquired in this study will be elaborated upon, as well as a discussion of what considerations should be made in regards to the grid codes. A discussion of additional research areas will also be clarified to highlight missing elements.

# 7 Discussion

This chapter will discuss the findings of this report divided into 4 sections discussing the different results obtained in this report

## 7.1 Model considerations

A few considerations need some additional elaboration, since the external grid is modeled as a single voltage source behind a Thevinin equivalent impedance. Where the voltage source does not have any form of control implemented, this implies that the model does not capture the interaction between different generators as it does not consider their participation factors in regards to PO damping. This simplification does reduce the validity of the developed control as it is not tested in an environment where controller interaction can occur.

Similarly, as the internal transmission path of the WPP have not been considered, and thereby internal losses and phase shift between the individual turbines have not been considered. And it has thereby not been investigated if the developed controller introduces to great a phase shift preventing a uniform response at the PCC. However, from the literature study in Section 2.3 on page 16, a very large WPP containing 150 WTGs was investigated where a phase shift of 14° and WPP still achieve a uniform response at the PCC. It is argued that the phase shift is of lesser concern as the baseline WPP used in this project only contains 91 WTGs.

Additionally, this study has applied many of the same simplifications as the studies listed in Table 2.2 on page 19 such as an aggregated WPP model, no consideration to the location of the PCC measurement, no modeling of grid meters. However, the goal was not to model several power system components but to develop a simple model that accounts for communication delay and the measurement delay between grid meters and WPP control and the individual WTGs that can be utilized to tune a POD controller after. However, these delays are extremely hardware-dependent, meaning the utilized time delay of 91 ms is an approximation that is not generally representative of all WPPs, and it has to be evaluated on a case-to-case basis.

Lastly, the considerations in regards to communication delays and measurement delays are approximations and will be dependent on the installed hardware at the physical location. Thus the time before the WPP starts acting upon any PO may be longer or shorter making it either easier or harder to comply with local grid codes.

## 7.2 Approximation of voltage at the PCC

The approach utilized in this study to predict the voltage at the PCC is derived based upon a two-bus system separated by an equivalent impedance and the standard power equations for computing power at the sending end bus. From this 4 solutions were found but, two are ruled out due to their negative sign. And a third solution was ruled out as it predicted the voltage to be far too low. Afterward, Equation 5.6 on page 36 accuracy was evaluated by varying the SCR and XR ratio and comparing it to a basic Gaus Siedel load flow solution to estimate its precision. From this investigation, it was found that this approach can only be used for stiff power grids ($SCR \geq 16$) and XR-ratio above 6.5. It is therefore argued that this approach should not be used for weak grids as there will be a significant difference between the load flow solution and Equation 5.6 on page 36 which could lead to faulty POD controller designs that do not acquire the desired damping.

However, for a stiff grid, this approach can be used to acquire a rough sketch to develop a controller, which later can be fine-tuned in a more detailed model.

## 7.3 The tuning process

The controller is tuned after an ideal power oscillation which is constructed after a standard second equation, where the desired damping, frequency, and amplitude are specified. It is approximated after a real event, thus the time frame of the oscillation and its behavior is controlled and not influenced by any dynamics. Therefore it is easy to tune a controller that performs well in the used simulation environment thus some care should be taken, and additional testing is needed to evaluate any controller tuned with this approach. It also has to be pointed out that it was decided that the POD controller should react upon amplitude power oscillation in apparent power and not reactive power directly, which may cause controller inaccuracies that are not accounted for in this study.

The POD controller was tuned with the assumption that the anti-phase could be achieved by inverting the given signal by multiplying it with -1. Anti-phase was achieved with this approach, however, it has not been investigated if the POD controller would achieve better performance by utilizing 3 lead-lag filters to acquire the desired anti-phase and damping. Utilizing 3 lead-lag filters would not alter the tuning process of pole and zero placement, but it will affect the stability of the controller as there are more pole and zero pairs that have to be placed in the left half-plane of the root locus diagram to achieve a stable controller. This in turn will also affect the gain of the controller, which may cause the controller to become more sensitive to frequencies outside its design frequency.

## 7.4 Controller performance, validation and grid codes

In both the Simulink model and the Simulink validation model damping was achieved with the POD controller, however, the results achieved are different from each other. Where adequate damping was achieved in the first model by increasing the rate limit the controller could react with implementing the same rate limit in the validation model resulted in periodic damping of the PO, but not close to adequate damping. This difference between the two models is argued to be caused by the difference that the validation model has an aggregated model of a WPP, which the POD controller stability signal is fed too whereafter it is translated to the WPP response as seen from the PCC. Where in the Simulink model it is assumed the output of the POD controller output represents the WPP response at the PCC. This clearly shows that the latter assumption is poor and should be neglected in the future. Additionally, in the Simulink model a saturation limit was not included therefore no considerations were given to the available power in the WPP meaning the controller could ask for more power than the available power, which should have been considered as it may have minimized the difference between the Simulink and the validation model.

The developed controller's performance is only evaluated for one power oscillation and one WPP power work point, which is a PO frequency of 0.29 Hz and a power working point of $P_{WPP}$=0.5 pu and $Q_{WPP}$=0.3 pu. It is therefore unknown how the controller behaves if exposed to a different power oscillation frequency or a different power level. Implying if the controller is given a different PO it may not achieve damping to the same degree, which should be investigated to ascertain the area in which the controller behaves as intended. It also has to be mentioned that the controller is only evaluated in the continuous-time domain, meaning the controller's stability and performance have not been evaluated in the Z-domain nor have there been given consideration to sampling time. This should be done in the future to achieve a controller design that is more applicable in the real world.

However, in both cases, the rate limit had to be changed to achieve damping and in both cases, it has to be increased over the tolerated limit in the grid codes. The time frame in which the control should be achieved was in both cases violated as the controller kept acting upon the PO after the 30-second mark. This indicates that if the power oscillation damping is to be achieved with WPPs that an exception in the grid codes should be considered. This, however, has to be done with care as fast-acting control may affecting the level of harmonics observed at the PCC which may affect power quality at the PCC. It may also impose additional strain on the power system components as it may ask for rapid current changes to achieve the desired power output.

Having elaborated upon the findings of this report a conclusion on the results will be made, and to see to what extend the study have been successful in answering the problem statement of Chapter 3

# 8 Conclusion and future works

This chapter summarizes the main conclusion based upon the result of this report whereafter it outlines topics for future works.

## 8.1 Conclusion

This report has attempted to answer the problem statement, which for simplicity is rewritten below:

*How to define a set of practical design criteria for an implementation of a WPP POD controller. Accounting for grid codes, time delays, and controller action.*

To answer this 3 sub-objectives were formulated which will be answered from 1 to 3. As the project did only model the grid meters as their imposed time delays it was found that in general can be represented with a time delay of 10 ms, but depending on the grid meter and the desired measurement this delay may be higher or lower. Therefore it is concluded that the time delay grid meters introduce should always be evaluated for each investigated case in regards to what hardware is being used. Concerning the 2'nd objective, no conclusion can be made as this investigation has not been conducted, and therefore it is a topic for future works. To evaluate what additional set of piratical design criteria can be proposed when the controller has to act in the entire inter-area frequency band. In regards to the 3'rd sub-objective, it is concluded that the developed controller does not provide adequate damping of the tested power oscillation of 0.29 Hz, but some damping is achieved. Indicating that additional research is needed to acquire a controller that provides adequate damping.

So only a partial answer to the main objective can be established as the 2'nd sub-objective remains to be answered.

It is concluded it is a difficult task to define a set of piratical design criteria, but some guidelines can be proposed from the work done in this report. However, the following can be concluded which partly answers the main objective. From the results obtained in chapters 5 and 6, it is concluded that the criteria of adequate damping of that the initial peak of the oscillation should be damped with 33% after 3'rd oscillation period although difficult to achieve should be maintained. It can also be concluded from the results that the current grid codes appear to be too tight to achieve power oscillation damping with WPPs and a different set of criteria is needed if WPP is to help with power oscillation damping in the future. Additionally, care must be shown to the different time delays internally in the WPP such as communication delay, measurement delay, and controller action. All of these delays should be approximated based on the utilized hardware to achieve an accurate representation of the phase shift the POD controller needs to provide to achieve the anti-phase. Thus it is proposed that the following checklist can be utilized to establish a set of initial design criteria on a case-to-case basis.

1. The phase shift the POD controller should provide, should be evaluated from the present time delay arising from measurements communication and controller action. This must be evaluated on a case-to-case basis to achieve the correct phase shift. In this report, it was estimated to be 91 ms which caused the needed phase shift to be 184.75°.
2. The POD controller should aim to dampen the initial power oscillation by 33% within 3 oscillation periods. The argument for this criteria is that if the controller is to be in some agreement with the time frame of the danish grid codes. However, it has to be mentioned that power oscillation of the inter-area nature can last longer than 30 seconds. So if WPPs are to participate in power oscillation damping the time frame in which the WPP must complete its control action for this specific control should be reevaluated.
3. The rate limit of the grid codes cannot be maintained if the following two points are to be achieved, and therefore if WPPs are to provide POD damping a reassessment of the rate limit of 10 MVA/s needs to be reconsidered. Meaning additional research is needed to establish a minimum needed rate limit to achieve adequate damping. This should also be evaluated on a case-to-case practice.
4. All though not investigated in this report, care should be taken in regards to the angle of separation between the WTGs does not rise to a level where a uniform response at the PCC is not possible when performing the POD control.
5. The POD controller design stability and performance should be evaluated in the discrete-time domain to ensure stable performance, to ascertain the effect of data sampling.
6. The effect of filtering should be investigated as the POD controller is not allowed to act outside the inter-area oscillation range.
7. Lastly, the POD controller needs to be evaluated over multiple frequencies to ensure it provides sufficient damping, to establish if additional filtering of the signal is needed, or if additional considerations must be given to the gain of the controller.

Lastly, it is concluded that the approach of approximating the grid as a voltage source behind an impedance is accurate enough to be used to create an initial controller design for stiff power grids. But special care must be shown if it is used for power grids whose SCR-ratio is below 16, and for an XR-ratio of less than 6.5 at the point of connection of the WPP.

## 8.2 Future works

This section outline topics for future research which is needed to achieve a more precise answer to how design criteria should be established for POD control performed by WPPs. The difference of additional topics of research needed to achieve a more precise answer is an outline in a bullet list.

- *It should be investigated if the POD controller achieves better performance by utilizing 3 lead-lag filters compared to achieving the antiphase by inverting the signal.*
- *The POD controller should be exposed to multiple PO at the same time to evaluate how it performs and to ascertain if additional filtering of the signal is needed for it to be able to dampen multiple PO's.*
- *The effect filtering has upon the POD controller should be investigated to ascertain if it introduces damping of the signal and how it affects the desired phase shift.*
- *The controller should be transferred into the Z-domain to evaluate its performance, stability and the effect of sampling has upon the POD controller.*
- *The POD controller should be implemented into the main control scheme of the WPP to investigate how the POD controller interacts with the different controllers in WPP such an AVR. To establish if additional design considerations need to be taken.*
- *The internal transmission path of the WPP should be modeled to investigate if the POD controller causes the angle of separation to become too great preventing the WPP from having a uniform response at the PCC.*

# Bibliography


[1] Prabha Khundur. *Power system stability and control.* MCGraw-Hill inc., 1'st edition, 1994. ISBN 0-07-035958-X.

[2] European Commission. *COMMUNICATION FROM THE COMMISSION TO THE EUROPEAN PARLIAMENT, THE COUNCIL, THE EUROPEAN ECONOMIC AND SOCIAL COMMITTEE AND THE COMMITTEE OF THE REGIONS.* `https://eur-lex.europa.eu/legal-content/EN/TXT/PDF/?uri=CELEX:52020DC0562&from=EN`, 2020. Last visited: 05/02/21.

[3] windeurope.org. Off-shore wind in europe. Technical report, Wind Europe, February 2021.

[4] Jun Bum Kwon senior Engineer at Energinet. *An INTRODUCTION TO THE DANISH POWER TRANSMISSION SYSTEM*, 2020. Last visited: 05/02/21.

[5] Bikash Pal Balarko Chaudhuri. *Robust Control In Power Systems.* Springer Science+Business Media Inc., 1'st edition, 2005. ISBN 978-0387-25949-9.

[6] E Grebe, J. Kabouris, S. López Barba, W. Sattinger, and W. Winter. Low frequency oscillations in the interconnected system of continental europe. *IEEE PES General Meeting*, 2010.

[7] H. Breulmann, E. Greve, M. Lösing, W. Winter, R. Witzmann, P. Dupuis, M.P. Houry, T. Margotin, J. Zerenyi, J. Dudzik, K. Martin, and J. Rodríguez. Analysis and damping of inter-area oscillations in the uscte/centrel power system. *Cigre 2000 Paper No 38-113*, 2000.

[8] O. Antoine, J-C. Maun, G. Jacobs, J. Warichet, and C. Druet. Inter-area Oscillation Monitoring Experience in Continental Europe and Study of the Power Flow Influence on Mode Damping. *INNOCATION FOR SECURE AND EFFICIENT TRANSMISSION GRIDS and CIGRÉ Belgium Conference*, 2014.

[9] Netbeheer Nederland. Power-generating modules compliance verification. Technical report, 2020.

[10] EirGrid. Eirgrid grid code version 9. Technical report, 2020.

[11] Energinet. Technical regulation 3.2.5 for wind power plants above 11 kw. Technical report, 2016.

[12] ENTSO-E. High penetration of power electronic interfaced power sources (HPOPEIPS). Technical report, 2017.

[13] National Grid Electricity System Operator. The grid code. Technical report, 2020.

[14] ENTSO-E. High penetration of power electronic interfaced power sources and th potential contribution of grid forming converters. Technical report, 2020.

[15] Zhixin Miao, Lingling Fan, Dale Osborn, and Subbaraya Yuvarajan. Control of DFIG-Based Wind Generation to Improve Interarea Oscillation Damping. *IEEE TRANSACTIONS ON Energy conversion*, vol. 24(2), June 2009.

[16] F. Michael Hughes, Olimpo Anaya-Lara, Nicholas Henkins, and Goran Strbac. Control of DFIG-Based Wind Generation for Power Network Support. *IEEE TRANSACTIONS ON POWER SYSTEMS*, vol. 20(4), November 2005.

[17] Jianhui Meng Yi Wnag, Xiangyu Zhang, and Lie Xu. Control of PMSG-Based Wind Turbines for system Inertial Response and Power Oscillation Damping. *IEEE TRANSACTIONS ON SUSTAINABLE ENERGY*, VOL 6(NO. 2), April 2015.

[18] Claudiu Ionita. Advanced Active Power and Frequency Control of Wind Power Plants. Master's thesis, Aalborg University, June 2017.

[19] Bachman. *Grid Measurement Modules.* `https://www.bachmann.info/en/products/controller-system/grid-measurement-module/`. Last visited: 14/03/21.

[20] Thyge Knüppel, Jørgen N. Nielsen, Kim H. Jensen, Andrew Dixon, and Jacob Østergaard. Power oscillation damping capacilities of wind power plant with full converter wind turbines considering its distributed and modular characteristics. *IET Renewable Power Generation*, December 2012.

[21] José Luis Domíngues-García, Oriol Gomis-bellmunt, Fernado D. Bianchi, and Andreas Sumper. Power Osillation damping supportted by Wind Power: A Review. *ELSEVIER Renewable and Sustainable Energy Reviews*, June 2012.

[22] Shaun Campbell. *Horns Rev 1, 2, 3: three generations of turbine output analysed.* `https://www.windpowermonthly.com/article/1663417/horns-rev-1-2-3-three-generations-turbine-output-analysed`, October 2019. Last visited: 14/03/21.

[23] Vattenfall. *Horns Rev 1.* `https://powerplants.vattenfall.com/horns-rev/`. Last visited: 22/04/21.

[24] State of Green. *Grid connection of Horns Rev 2 200 kV offshore wind farm.* https://stateofgreen.com/en/partners/energinetdk/solutions/grid-connection-of-horns-rev-2-200-kv-offshore-wind-farm/. Last visited: 22/04/21.

[25] L. Petersen and F. Iov. Practical Considerations Regarding Implementation of Wind Power Applications into Real-Time Hardware-In-The-Loop Framework.

[26] Bryan d'Emil, Morten Jacobsen, Martin Starcke Jensen, Søren Krohn, Kim Conrad Petersen, and Katrine Sandstroem. *Wake Effect.* http://www.xn--drmstrre-64ad.dk/wp-content/wind/miller/windpower%20web/en/tour/wres/wake.htm. Last visited: 28/04/21.

[27] A. Bhatia. *Basic Electrical Engineering for HVAC Engineers.* https://www.cedengineering.com/userfiles/Basic%20Eectrical%20Engineering%20for%20HVAC%20Engineers.pdf. Last visited: 05/02/21.

[28] P.E. Christopher L. Brooks. *An Overview of Wind Plant Design Standards and Common Nomenclature Available Resources to the Power Engineer.* https://www.ieee-pes.org/presentations/td2014/td2014p-000646.pdf. The author is a senior memeber of IEE and a pricipal-manager at ESC engineering inc. Last visited 01/08/21.

[29] Jan Machowski, Janus W. Bialek, and James R. Bumby. *POWER SYSTEM DYNAMICS Stability and Control.* John Wiley & Sons, Ltd, 2nd edition, 2008. ISBN: 978-0-470-72558-0.

[30] Lennart Petersen and Fitim Kryezi. Wind Power Plant Control Optimisation with Embeded Application of Wind Turbines and STATCOMs. Master's thesis, Aalborg University, June 2015.

[31] Allan-Bradley. *Grid Measurement Modules.* https://www.rockwellautomation.com/en-us/products/hardware/allen-bradley/energy-monitoring.html. Last visited: 14/03/21.

[32] Beckhoff. *Grid Measurement Modules.* https://www.beckhoff.com/en-us/products/i-o/power-measurement/. Last visited: 14/03/21.

[33] Mohamed A. Ahmed and Young-Chon Kim. Communication Network Architectures for Smart-Wind Power Farms. *Energies*, June 2014. ISSN 1996-1073.

[34] ENerginet. Technical regulation 3.2.3 for thermal power plants above 11 kw. Technical report, July 2016.

[35] Entsoe. *Oscillation Event 03.12.2017 System Protection and Dynamics WG*, March 2018.

[36] *THE DOCTORAL SCHOOL OF ENGINEERING AND SCIENCE.*
https://www.phd.engineering.aau.dk/. Last visited: 13/07/21.

# A | Appendix A

| XR | 6.5 | 7 | 7.5 | 8 | 8.5 | 9 | 9.5 | 10 |
|---|---|---|---|---|---|---|---|---|
| SCR | Percentage Error Between Load Flow and Equation 5.5 | | | | | | | |
| 15.6 | 0.552 | 0.514 | 0.481 | 0.452 | 0.426 | 0.403 | 0.382 | 0.363 |
| 15.8 | 0.545 | 0.508 | 0.475 | 0.446 | 0.420 | 0.398 | 0.377 | 0.359 |
| 16 | 0.539 | 0.501 | 0.469 | 0.441 | 0.415 | 0.393 | 0.373 | 0.354 |
| 16.2 | 0.532 | 0.495 | 0.463 | 0.435 | 0.410 | 0.388 | 0.368 | 0.350 |
| 16.4 | 0.526 | 0.489 | 0.458 | 0.430 | 0.405 | 0.383 | 0.364 | 0.346 |
| 16.6 | 0.519 | 0.484 | 0.452 | 0.425 | 0.400 | 0.379 | 0.359 | 0.342 |
| 16.8 | 0.513 | 0.478 | 0.447 | 0.420 | 0.396 | 0.374 | 0.355 | 0.338 |
| 17 | 0.507 | 0.472 | 0.442 | 0.415 | 0.391 | 0.370 | 0.351 | 0.334 |
| 17.2 | 0.501 | 0.467 | 0.437 | 0.410 | 0.387 | 0.366 | 0.347 | 0.330 |
| 17.4 | 0.496 | 0.462 | 0.432 | 0.406 | 0.382 | 0.362 | 0.343 | 0.326 |
| 17.6 | 0.490 | 0.456 | 0.427 | 0.401 | 0.378 | 0.357 | 0.339 | 0.322 |
| 17.8 | 0.485 | 0.451 | 0.422 | 0.397 | 0.374 | 0.353 | 0.335 | 0.319 |
| 18 | 0.480 | 0.446 | 0.418 | 0.392 | 0.370 | 0.350 | 0.332 | 0.315 |
| 18.2 | 0.474 | 0.442 | 0.413 | 0.388 | 0.366 | 0.346 | 0.328 | 0.312 |
| 18.4 | 0.469 | 0.437 | 0.409 | 0.384 | 0.362 | 0.342 | 0.324 | 0.309 |
| 18.6 | 0.464 | 0.432 | 0.404 | 0.380 | 0.358 | 0.338 | 0.321 | 0.305 |
| 18.8 | 0.459 | 0.428 | 0.400 | 0.376 | 0.354 | 0.335 | 0.318 | 0.302 |
| 19 | 0.455 | 0.423 | 0.396 | 0.372 | 0.350 | 0.331 | 0.314 | 0.299 |
| 19.2 | 0.450 | 0.419 | 0.392 | 0.368 | 0.347 | 0.328 | 0.311 | 0.296 |
| 19.4 | 0.445 | 0.415 | 0.388 | 0.364 | 0.343 | 0.325 | 0.308 | 0.293 |
| 19.6 | 0.441 | 0.410 | 0.384 | 0.360 | 0.340 | 0.321 | 0.305 | 0.290 |
| 19.8 | 0.436 | 0.406 | 0.380 | 0.357 | 0.336 | 0.318 | 0.302 | 0.287 |
| 20 | 0.432 | 0.402 | 0.376 | 0.353 | 0.333 | 0.315 | 0.299 | 0.284 |

Table A.1: Error between predicted voltage by Equation 5.6 and load flow solution

# B | Appendix B: PO generation

```
%%%%%%%%%%%%%%%%%%%%%%%%%%%%%%%%%%%%%%%%%%%%%%%%%%%%%%%%%%%%%%%%%%%%%%%%%
% intialization
Tw= 10;
T1=0.075;
T2=0.029;
EVg=400*10^3;%V
Prated=209*10^6; % W
Grid.SCR=20;
Grid.XR=10;
Fbase=50;
Zbase=EVg^2/(Prated*Grid.SCR);
Sbase=Prated*Grid.SCR;
% the different gains

K2=1.00768;
K3=1;
% injected power in MW
P=(0.5*Prated)/Sbase; % converting the injected power
                      % by the WPP to the power base of the grid.
% grid impedance

Zg= EVg^2/(Sbase); % ohms

Zgsim=Zg/Zbase;

Rg=(Zg*cos(atan(Grid.XR)))/Zbase; % per unit impedance
Xg=(Zg*sin(atan(Grid.XR)))/Zbase;

Rg1=(Zg*cos(atan(Grid.XR))); %in ohms
Xg1=(Zg*sin(atan(Grid.XR)));

%computing inductance  fbase = 50 Hz
Xg1L=Xg1/(2*pi*50);


ZgComplex=complex(Rg,Xg);
ZgComplex1=complex(Rg1,Xg1);

Zgabs=abs(ZgComplex);
Zgabs1=abs(ZgComplex1);


%initializing s as laplace
s=tf('s') % transfer function

% initializing time, frequency and damping
omega=0.29*2*pi;
zeta=0.010;
t = (0:0.005:65);

%initializing the step options
opt = stepDataOptions;
opt.StepAmplitude = 0.0475;
opt.InputOffset =(-0.0475);
%opt.StepTime=1;
```

```
% The signal
PO=(omega^2)/(s^2+(2*zeta*omega*s)+omega^2);

y1=step(PO,t,opt); % oscillation

%the math used to compute V PO to Q PO ideally.

y2=y1+1; % grid voltage in pu
y3=(y2./ZgComplex); % grid current in pu
y4=y3.*y2; % apperent power
y5=abs(imag(y4)); % Q
```

# C | Appendix C:Validation initialization script

```
% clear all
% clc

SCR = 20;
XpR = 10;
Pbase_WPM = 104.5; %MW
Pbase_PVPM = 104.5; %MW
Prated=209; %MW

Phpp = Pbase_WPM+Pbase_PVPM; %MW
%Base Power
Pbase =  SCR * Phpp; %[MW]
%Base Voltage
Vbase = 400; %[kV] line
Vbase_initialize=(325*10^3) %phase to ground voltage
%Base Impedance
Zbase = Vbase^2 / Pbase;
%Frequency
Fbase = 50;
%Initial Phase of voltage
PhaseV = 0;


%%%%%%%%%%%%%%%%%%%%%%%%%%%%%%%%%%%%%%%%%%%%%%%%%%%%%%%%%%%%%%%%%%%%%%%%%%%%%%
%Grid impedance [ohms]
Zgrid = Vbase^2 / Pbase;
%Grid Resistance [ohms]
Rgrid = Zgrid * cos(atan(XpR))



%Grid Reactance [ohms]
Xgrid = Zgrid * sin(atan(XpR))

Lgrid = Zgrid * sin(atan(XpR))/(2*pi*Fbase) %henry

%Grid impedance in complex [ ohms]

Zcomplex=complex(Rgrid,Xgrid)

%%%%%%%%%%%%%%%%%%%%%%%%%%%%%%%%%%%%%%%%%%%%%%%%%%%%%%%%%%%%%%%%%%%%%%%%%%%%%%

%Transformations
ABC2AlphaBeta = 2/3 * [1 -0.5 -0.5;0 sqrt(3)/2 -sqrt(3)/2];
AlphaBeta2ABC = 3/2 * [2/3 0; -1/3 sqrt(3)/3; -1/3 -sqrt(3)/3];

%Frequency Profile
Tset = 1;
zeta=0.010;
omgn = 0.29*2*pi;

Num = [ 0 omgn^2];
Den = [1 2*zeta*omgn omgn^2];
Tf = 10e-3;
```

```
% controller parameter

Kg=1.00789;
Tw= 10;
T1=0.075;
T2=0.029;
```